Journal of Water Process Engineering 59 (2024) 105042

Contents lists available at ScienceDirect

Journal of Water Process Engineering

journal homepage: www.elsevier.com/locate/jwpe

Calcium silicate solid-state matrices from boric acid production waste for ^{60}Co removal and immobilization by spark plasma sintering

O.O. Shichalin [a,*], S.B. Yarusova [b,c], N.P. Ivanov [a], E.K. Papynov [a], A.A. Belov [a], S.A. Azon [a], I.Yu Buravlev [a], A.V. Myagchilov [a], A.N. Fedorets [a], V.L. Rastorguev [a], Ya.G. Zernov [a], S.Yu. Budnitskiy [d], V.Yu Mayorov [a,d], E.A. Gridasova [a], I.G. Tananaev [a,e], A.I. Ivanets [f,*], P.S. Gordienko [b]

[a] Far Eastern Federal University, 10 Ajax Bay, Russky Island, Vladivostok 690922, Russia
[b] Institute of Chemistry, Far Eastern Branch of Russian Academy of Sciences, 159, Prosp. 100-letiya Vladivostoka, Vladivostok 690022, Russia
[c] Vladivostok State University of Economics and Service, Gogolya st., 41, Vladivostok 690014, Russia
[d] Far East Geological Institute, Far Eastern Branch of Russian Academy of Sciences, 159, Prosp. 100-letiya Vladivostoka, Vladivostok 690022, Russia
[e] Kola Science Centre, Russian Academy of Sciences, 14 Fersman Street, Apatity 184200, Russia
[f] Institute of General and Inorganic Chemistry of National Academy of Sciences of Belarus, Surganova St. 9/1, Minsk 220072, Belarus

ARTICLE INFO

Keywords:
Calcium silicate
^{60}Co adsorption
Ceramic matrices
Spark plasma sintering
Waste-to-waste

ABSTRACT

A mesoporous adsorbent based on calcium silicate $CaSiO_3$ for the removal and immobilization of cobalt ^{60}Co radionuclides in durable ceramic $CaCoSi_2O_6$ matrices was synthesized by hydrothermal conversion of boric acid production waste. The obtained material had a high Co^{2+} ions adsorption capacity of 220.8 mg/g. Cobalt adsorption was carried out mainly by ion exchange, which led to the formation of $CaCoSi_2O_6$ precursor ceramic matrices. The use of spark plasma sintering (SPS) technology at an optimal temperature of 1000 °C allowed the safe immobilization of Co^{2+} ions in $CaCoSi_2O_6$ ceramic matrices characterized by density (3.33 g/cm^3), compressive strength (481 MPa) and microhardness (~9.81 GPa). Sintered $CaCoSi_2O_6$ ceramic samples were characterized by high hydrolytic stability (cobalt leaching rate R_{Co} ~10^{-7} g/(cm^2 × day)) and complied with the requirements for cured highly active waste GOST R 50926 96/ANSI/ANS 16.1.

1. Introduction

^{60}Co a radioactive isotope of cobalt that is formed in nuclear reactors as a byproduct of the neutron activation of the corrosion products of structural materials containing significant amounts of iron (stainless steel or other iron-based alloys). The formation of ^{60}Co occurs through a sequence of neutron capture reactions, each followed by radioactive decay [1–3]. The presence of ^{60}Co in liquid nuclear waste (LRW), poses a challenge for waste management and long-term storage. Ensuring the safe containment and sequestration of ^{60}Co is of paramount concern, as improper disposal can lead to the spread of radioactive contamination, posing severe risks to ecosystems and human populations. Consequently, the development of effective strategies for the extraction and subsequent immobilization of radioactive cobalt has become a vital area of research. In addition, the development of materials for the removal of stable isotopes of cobalt from liquid media is an extremely important scientific task, due to the high toxicity of this heavy metal [4–7].

The functional materials belonging to the organic and inorganic adsorbents are widely used for the selective removal of Co^{2+} ions, both in macroconcentration (for wastewater treatment from heavy metals) and in trace concentration (for LRW purification from ^{60}Co radionuclides) [8–13]. Thus, multifunctional adsorbents based on sodium titanate had an adsorption capacity of 50.2 mg/g [11]. Chitosan-based organic polymer adsorbents were prepared for the selective removal of Co^{2+} ions and had adsorption capacity of 0.265 mmol/g [10]. A carbon dot/chitin nanocrystal hybrid adsorbent could remove Co^{2+} up to 152 mg/g [12]. Radiation-grafted chitosan adsorbent could capture of an extremely high amount Co^{2+} of 421 mg/g [13]. The functionalized polymeric thiocarbamate adsorbent had an adsorption capacity of 0.47 mmol/g [8]. Composite Ti-Ca-Mg phosphates had an adsorption capacity of 86 mg/g and high distribution coefficients $K_d(^{60}Co) = 38.30 \times 10^5$ ml/g during ^{60}Co radionuclides adsorption from multicomponent

* Corresponding authors.
E-mail addresses: shichalin_oo@dvfu.ru (O.O. Shichalin), ivanets@igic.bas-net.by (A.I. Ivanets).

https://doi.org/10.1016/j.jwpe.2024.105042
Received 8 November 2023; Received in revised form 11 February 2024; Accepted 20 February 2024
Available online 24 February 2024

LRW [9].

Inorganic adsorption materials (especially silicate and aluminosilicate adsorbents) have a number of advantages in removing heavy metal cations (including Co^{2+}, Pb^{2+}, Zn^{2+}) and radionuclides (^{137}Cs, ^{90}Sr, ^{60}Co) from liquid media. Such advantages include high adsorption capacity, high selectivity, possibility of regeneration, radiation and chemical resistance, low cost of production, and high adsorption kinetics [14–20]. Mesoporous layered calcium silicate $CaSiO_3$, obtained from coal fly ash, had a high adsorption capacity to Co^{2+} of 154.8 mg/g and was capable of removing up to 99.9 % of ^{60}Co radionuclide under real LRW purification conditions with an initial activity of ^{60}Co A_0 = 5.14 kBq/l. Granular porous zirconium silicate synthesized in the framework of the study had an adsorption capacity of 0.84 mmol/g [21]. Zirconium molybdenum silicate adsorbent had an adsorption capacity of $q(Co^{2+})$ = 47.4 mg/g and selectivity to Co^{2+} ions in a tertial system of Cs-Sr-Co [22].

The adsorption of Co^{2+} ions from liquid media on silicate sorption materials of various phase compositions proceeded mainly through mechanisms of ion exchange and surface complexation of an intra- and innerspheric interaction [23–26]. The mechanism of Co^{2+} ions adsorption on mesoporous calcium silicate includes the following steps: (1) hydration of Co^{2+} ions to form $Co(H_2O)_6^{2+}$ (up to 99.79–100 %), (2) diffusion of hydrated cobalt ions through the boundary layer, (3) complexation with active groups on the surface of calcium silicate >SiOH and >CaOH and ion exchange with Ca^{2+} ions adsorbed on the surface and edges of the particles, (4) diffusion into the inner layer of the material and ion exchange with Ca^{2+} ions (up to 76.7 % of cobalt ions are adsorbed by ion exchange) [26].

Due to the course of cobalt adsorption by ion exchange mechanism and surface complexation, silicate and aluminosilicate adsorbents of various types can be regenerated after adsorption saturation with heavy metal ions (Co^{2+}, Ni^{2+}), which opens up prospects for their industrial application in multiple adsorption-desorption cycles [22,27–30]. Thus, the effective desorption of Co^{2+} ions (92.05 %) by adsorption material based on mixed metal silicate using 0.1 M HCl solution was showed [22]. The possibility of using clinoptilolite based zeolite-geopolymer foams and metaceolite obtained from natural raw materials to remove Ni^{2+} ions followed by regeneration with 0.1 M HNO_3 solution was studied [29]. The use of natural clinoptilolite as adsorbent for Ni^{2+} ions removal was discussed [28]. It was shown that the modified natural material had adsorption capacity in the range of 24–28 mg(Ni^{2+})/g and can be efficiently regenerated using NH_4Cl (desorption degree of Ni^{2+} reached 98 %), Na_2EDTA (~84 %), HNO_3 (~66 %), HCl (~59 %). Nanostructured adsorption material based on natural zeolite immobilized in a chitosan matrices retained the adsorption capacity to nickel of 40 mg/g after 5 cycles of adsorption-desorption regeneration at an initial adsorption capacity of 43 mg/g [27].

In addition, adsorbents based on silicates and aluminosilicates can be not only regenerated, but also directly used as matrices for the immobilization of dangerous ^{137}Cs, ^{90}Sr, ^{60}Co radionuclides and toxic Pb^{2+}, Co^{2+} heavy metal ions [31–36]. During the heat treatment of saturated adsorbents, stable ceramic matrices was crystallized, which reliably keep radionuclide and heavy metal cations from being released into the environment [37–40].

Previously, we studied synthetic calcium silicate, a very potent adsorbent with a adsorption capacity of 195.7 mg/g to Co(II) [41]. Using the spark plasma sintering (SPS) consolidation method, we were able to immobilize adsorbed cobalt ions quickly and efficiently into a strong ceramic wollastonite matrix. SPS is carried out by applying a pulsed direct current through the powder mass simultaneously with mechanical action, generating localized joule heating and spark discharges at the interface between particles [42,43]. This process leads to rapid heating and enables sintering to occur at lower temperatures and for shorter periods of time than conventional methods. Combining this with uniaxial pressure ensures high densification and improved grain boundaries [44,45]. The obtained matrices met the requirements for solid radioactive waste.

In this work, we propose a new method for obtaining calcium silicate matrices for cobalt immobilization, involving the hydrothermal conversion of boric acid production waste and subsequent consolidation of cobalt-calcium silicate by SPS. Previously, we optimized the conditions for calcium silicate formation from boric acid waste and studied the kinetics of heavy metals adsorption on calcium silicate from boric acid waste [46–48].

Boric acid (H_3BO_3) has a variety of applications due to its unique chemical properties, including glass and ceramics manufacturing, flame retardants, metalworking, insecticides and pest control, antiseptics, and the nuclear industry [49]. In Russia, limited liability company (LLC) «DHK Bor» is the leading national producer of boric acid with an output of 89,600 tons of products per year. The technological process of obtaining boric acid, implemented on LLC «DHK Bor», involves the reaction of the datolite mineral $CaBSiO_4(OH)$) with sulfuric acid. As a result of this technological process, boric acid is obtained, and insoluble waste, known as borogypsum, is precipitated. The main components of borogypsum, obtained from datolite reprocessing are hydrate calcium sulfate ($CaSO_4$ $2H_2O$) and amorphous silica (SiO_2). Reprocessing borogypsum is necessary to mitigate waste disposal issues and recover valuable resources. Most of the scientific studies involving borogypsum reprocessing originate from Turkey, which is one of the leaders in boron acid production. It is proposed to use borogypsum as a building material and as a protection against ionizing radiation [50–53]. However, the Turkish process for obtaining boric acid involves the usage of the colemanite mineral $CaB_3O_4(OH)_3{\cdot}H_2O$, which has a low content of silicon [54]. In this regard, we have developed an original method for the processing of borogypsum, obtained from minerals with a high silicon content.

The work aimed to evaluate the possibility of using silicate matrices obtained by hydrothermal conversion of boric acid production waste for cobalt immobilization. For this, calcium silicate was synthesized from the waste products of boric acid production. Cobalt-saturated calcium silicate samples were consolidated using the SPS method. The most important properties of ceramic matrices, such as the surface morphology, strength, hardness, phase and elemental composition, and cobalt leachability, were carefully studied.

The scientific novelty of the work is as follows: (i) an original method for the immobilization of cobalt ions into a durable ceramic matrices and the simultaneous reprocessing of boric acid waste is proposed; (ii) for calcium silicate obtained from boric acid production wastes, the surface area and its morphology, pore sizes and shapes, particle sizes, as well as adsorption properties to Co(II) are determined; (iii) for ceramic matrices of Co-saturated calcium silicate, consolidated by the SPS method at different temperatures (800, 900 and 1000 °C), their strength, hardness, density, chemical composition, phase composition, and resistance to cobalt leaching were determined; (iv) the efficient waste-to-waste technology is proposed.

2. Experimental

2.1. Materials and reagents

Samples of solid waste from the production of boric acid were taken from the sludge storage facility of DHK Bor LLC (Dalnegorsk, Russian Federation).

The following reagents were used: potassium hydroxide KOH, hydrochloric acid HCl, cobalt (II) chloride hexahydrate $CoCl_2{\cdot}6H_2O$. All chemicals were purchased from Nevareaktiv LLC (Saint-Petersburg, Russian Federation) at 99.9 % purity without additional purification.

2.2. Synthesis of $CaSiO_3$ from boric acid waste

The process of obtaining calcium silicate adsorbent from boric acid production waste in the presence of an alkaline agent (potassium hy-

droxide) is described by the following eq. [47]:

$$n(CaSO_4 \cdot 2H_2O) + m(SiO_2 \cdot qH_2O) + 2nKOH + (k - 3n - mq)H_2O = nCaO \cdot mSiO_2 \cdot kH_2O + nK_2SO_4 \quad (1)$$

Carrying out the reaction in the presence of atmospheric air leads to the occurrence of a side reaction with carbon dioxide and the partial formation of calcium carbonate in the synthesis product [46]:

$$Ca(OH)_2 + CO_2 \rightarrow CaCO_3 + H_2O \quad (2)$$

An accurate weight of solid powdery waste from the production of boric acid was placed in a KOH solution in distilled water. The reagents were taken in a stoichiometric ratio. The resulting suspension was thoroughly mixed and transferred into a Teflon beaker, which was placed in a steel vessel for hydrothermal synthesis. The synthesis was carried out at a pressure of 1.7 atm for 2 h. The precipitate was separated from the solution by vacuum filtration using a blue-ribbon filter, thoroughly washed with distilled water, and dried to constant weight at a temperature of 105 °C.

To determine the degree of reaction progress, the residual concentration of KOH in the solution was determined by acid–base titration with 0.01 M HCl and a methyl orange indicator. The extent of the reaction under the specified conditions is 81.2 %.

A schematic diagram of the process of obtaining the material, indicating side reactions leading to the presence of impurities of calcite and vaterite in the samples of synthesized calcium silicate, is presented in Fig. 1.

2.3. Adsorption characteristics of $CaSiO_3$ material

The adsorption characteristics of the $CaSiO_3$ material for Co^{2+} ions were studied using batch adsorption experiments. The ratio of liquid phase to solid phase was V/m = 40 ml/g (the volume of the $CoCl_2$ solution was 20 ml, and the mass of the adsorbent was 0.5 g). The temperature of water solutions was 20 °C and the pH was 6.2. As a source of cobalt ions, cobalt chloride $CoCl_2$ was used without a background electrolyte. The initial concentrations of Co^{2+} ions were 4.27–28.0 mmol/l. For a typical experiment, the suspension of an adsorbent in a cobalt solution was put on a magnetic stirrer RT 15 power (IKA, Germany) for 3 h. After adsorption, the phases were separated by filtration through a paper filter (pore size 2–3 μm). The content of Co^{2+} ions in the initial solutions and filtrates after adsorption was determined by atomic absorption spectrometry (AAS) on an AA-6800 spectrometer (Shimadzu, Japan) with a wavelength of 240.7 nm. The detection limit for cobalt in aqueous solutions is 0.1 μg/ml.

The adsorption capacity q (mmol/g) was determined using Eq. (3):

$$q_{eq} = (C_0 - C_1)\frac{V}{m}, \quad (3)$$

where q_{eq} – static exchange capacity, mg/g; C_0 – initial adsorbate concentration, mg/l; C_1 – adsorbate concentration after adsorption, mg/l; V – liquid phase volume, l; m – mass of the solid phase, g.

For mathematical processing of the experimental data of adsorption isotherms, the well-known models of adsorption at the solid/liquid interface were used: Freundlich isotherm, Langmuir isotherm and Langmuir-Freundlich isotherm.

The Freundlich isotherm model is expressed by the Eq. (4):

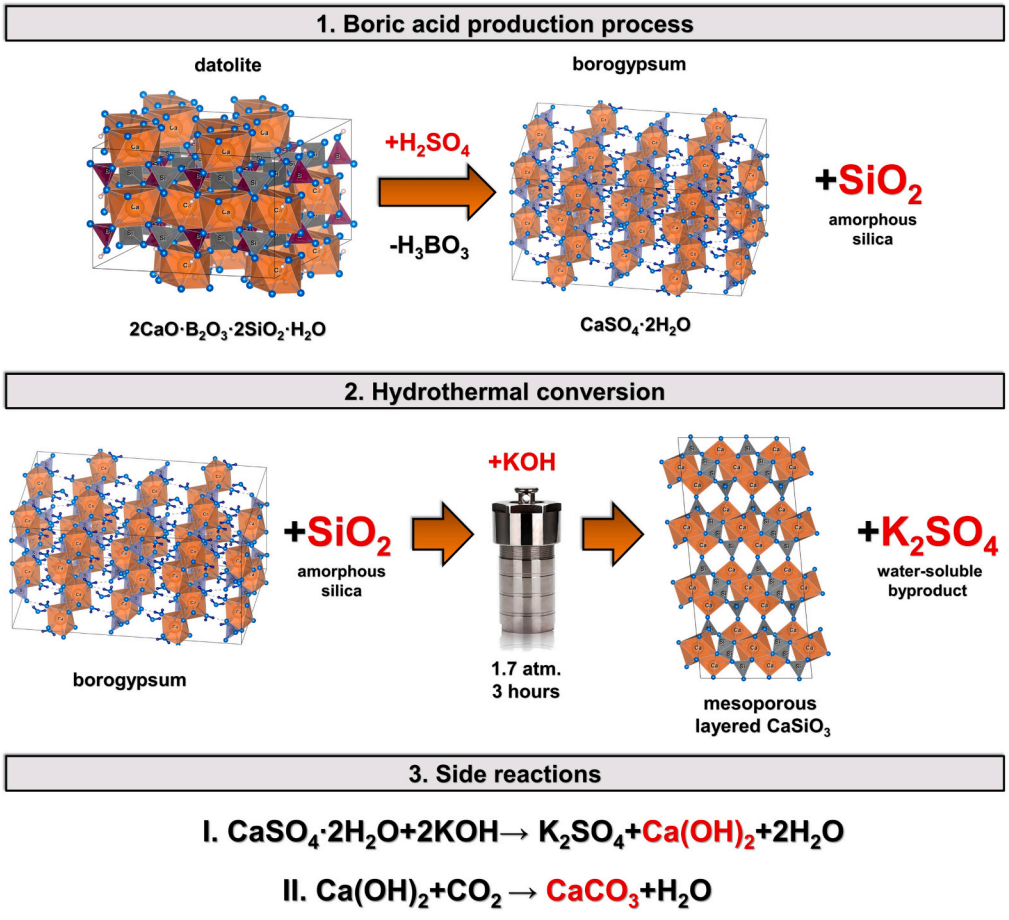

Fig. 1. Schematic diagram of the synthesis processes of calcium silicate adsorbent.

$$q_{eq} = K_f C_{eq}^n, \quad (4)$$

where q_{eq} – static exchange capacity, mg/g; K_f – Freundlich constant; C_{eq} – equilibrium concentration of the adsorbate, mg/l; n – Freundlich power factor.

The Langmuir isotherm model is expressed by the Eq. (5):

$$qeq = q_{max}^l \frac{K_l C_{eq}}{1 + K_l C_{eq}}, \quad (5)$$

where q_{eq} – static exchange capacity, mg/g; q_{max}^l – theoretical maximum adsorption capacity, mg/g; K_l – Langmuir constant, C_{eq} – equilibrium concentration of the adsorbate, mg/l.

To approximate the results of the experiment by the Langmuir-Freundlich model, the following equation was used:

$$qeq = q_{max}^{lf} \frac{K_{lf} C_{eq}^m}{1 + K_{lf} C_{eq}^m}, \quad (6)$$

where qeq – static exchange capacity, mg/g; q_{max}^{lf} – theoretical maximum adsorption capacity, mg/g, K_{lf} – Langmuir-Freundlich constant, C_{eq} – equilibrium concentration of the adsorbate, mg/l; m – Langmuir-Freundlich power factor.

Approximation of the experimental data by the indicated equations in a non-linear form was carried out using the OriginLab program.

To assess the accuracy of the description of experimental data by adsorption isotherm models, four different error functions were used: Pearson fitting criterion χ^2, mean square error (MSE), sum of square errors (SSE), hybrid fractional errors (HYBRID) [55–57]. These functions are expressed by the following equations:

$$\chi^2 = \sum_{i=1}^{n} \frac{\left(q_e^{exp} - q_e^{cal}\right)^2}{q_e^{cal}}, \quad (7)$$

$$MSE = \frac{1}{n} \sum_{i=1}^{n} \left(q_e^{exp} - q_e^{cal}\right)^2, \quad (8)$$

$$HYBRID = \frac{100}{n-p} \sum_{i=1}^{n} \frac{q_e^{exp} - q_e^{cal}}{q_e^{exp}}, \quad (9)$$

$$SSE = \sum_{i=1}^{n} \left(q_e^{exp} - q_e^{cal}\right)^2, \quad (10)$$

where n – number of the experiments, p – number of the model parameters, q_e^{exp} – experimental equilibrium adsorption capacity, mmol/g; q_e^{cal} – calculated adsorption capacity, mmol/g.

2.4. Adsorption saturation of $CaSiO_3$ material

Adsorption saturation of $CaSiO_3$ adsorbent with Co^{2+} ions was performed via batch adsorption. The ratio of liquid phase to solid phase was V/m = 40 ml/g (the volume of the $CoCl_2$ solution was 400 ml, and the mass of the adsorbent of 10.0 g) at pH of 6.2 and aqueous solution temperature of 20 °C. As a source of cobalt ions, cobalt chloride $CoCl_2$ with the initial concentration of 280 mmol/l was used without a background electrolyte. The suspension of a adsorbent in a cobalt solution was put on a magnetic stirrer RT 15 power (IKA, Germany) for 3 h. Then the precipitate was separated from the solution by vacuum filtration using a paper filter (pore size of 2–3 μm), thoroughly washed with distilled water, and dried to a constant weight at a temperature of 105 °C. The $CaCoSi_2O_6$ material saturated with cobalt ions Co^{2+} was used to obtain ceramic solid-state matrices.

2.5. Spark plasma sintering of $CaCoSi_2O_6$ solid-state matrices

The synthesis of the ceramic matrices was carried out by the SPS method by consolidating the resulting powder on an SPS-515S device, (Dr.Sinter LABTM, Japan). 1 g of the powder was placed in a graphite mold (working diameter 10.5 mm), then the workpiece was transferred to a vacuum chamber (10–5 atm.) and sintered. A series of samples was obtained at consolidation temperatures of 800, 900, and 1000 °C, a heating rate of 170 °C/min, a constant load of 24.5 MPa, and a retention time of 5 min. The geometric dimensions of the obtained samples of cylindrical matrices are: diameter 10.3 mm, height 4–5 mm (depending on the type of mold and sintering modes).

2.6. Characterization of powder materials and ceramics matrices

The phase composition of the obtained samples were identified using X-ray diffraction analysis (XRD) on an X-ray diffractometer D8 Advance Bruker-AXS (Bruker, Germany), CuKα radiation, Ni filter, average wavelength (λ) of 1.5418 Å, shooting angle range of 10–80°, scanning step of 0.02°. The beam was detected by the Vantec-1 linear detector with step of 0.00622127° (0.0031°) (unchanged parameter).

The particle sizes were determined using a NanoTec/MicroTec/XT Analysette-22 (FRITSH, Germany).

Determination of the specific surface area, pore volume and pore diameter distribution of sodium aluminosilicate samples was carried out using an Autosorb-IQ specific surface analyzer (Quantachrome, USA).

The thermogravimetric curves were recorded on the DTG-60H Shimadzu device in platinum crucibles with a pierced lid in a dry argon stream (20 ml/min) in the temperature range of 35–1300 °C at the heating rate of 10 °C/min (Shimadzu, Japan).

Scanning electron microscopy (SEM) on a Carl Zeiss ULTRA 55 Plus instrument (Germany) was used to obtain images of the surface of the material under study. To determine the elemental composition of the samples, we used energy dispersive X-ray spectroscopy (EDX) using an attachment to an Oxford X Max 80 electron microscope (United Kingdom) and X-ray fluorescence analysis (XRF) on a Shimadzu EDX-7000P energy dispersive X-ray fluorescence spectrometer (Japan).

Fourier transform infrared (FTIR) absorption spectra were recorded on a Fourier transform spectrophotometer “Iraffinity-1S” (“Shimadzu”, Japan).

Vickers microhardness (HV) was determined with a load of 0.2 N on an instrument HMV-G-FA-D (Shimadzu, Japan). The experimental density was determined by hydrostatic weighing using an Adventurer instrument (OHAUS Corporation, USA). The compressive strength was determined using an Autograph AG-X plus 100 kN tensile testing machine (Shimadzu, Japan).

2.7. Evaluation of metal ions leaching from $CaCoSi_2O_6$ silicate matrices

The leaching rate of cobalt ions was measured under static conditions for 30 days in distilled water (at pH 6.8) at room temperature (25 °C) in accordance with the Russian State Standard (GOST R 52126–2003), compiled according to the requirements of the American National Standards Institute/American Nuclear Society 2019 (ANSI/ANS 16.1) and an earlier IAEA recommended document (ISO 6961:1982). The content of Co^{2+} ions in the initial solutions and filtrates after adsorption was determined by AAS on an AA-6800 spectrometer (Shimadzu, Japan) with a wavelength of 240.7 nm. The detection limit for cobalt in aqueous solutions is 0.1 μg/ml.

The effective diffusion coefficient D_e was calculated according to Fick’s second law in accordance with the method described in [58]:

$$\frac{\sum m}{M_0} = 2 \left(\frac{D_e}{\pi}\right)^{\frac{1}{2}} \left(\frac{S}{V}\right) t^{\frac{1}{2}} + \alpha, \quad (11)$$

where m – mass of cobalt leached from the sample, mg; t – leaching time, s; M_0 – initial mass of cobalt in the sample, mg; D_e – effective diffusion coefficient, cm^3/s, S – sample surface area, cm^2, V – sample volume, cm^3, α – initial leaching constant.

To calculate the diffusion coefficient, the above equation was presented in a linear form by introducing the coefficient K, which is the tangent of the slope of the dependence of the leached fraction of cobalt on the square root of the contact time of the material with the leaching agent:

$$K = 2\left(\frac{D_e}{\pi}\right)^{0.5}\cdot\left(\frac{S}{V}\right), \quad (12)$$

According to the linear form of the equation, the effective diffusion coefficient was calculated using the following Eq. (13):

$$D_e = \frac{K^2\cdot\pi}{4}\cdot\left(\frac{V}{S}\right)^2, \quad (13)$$

The dominant leaching mechanism was determined based on the dependence of the decimal logarithm of the accumulated fraction of the leached radionuclide (Bt, mg/m^2) on the decimal logarithm of the leaching time (t, s):

$$lg(B_t) = \frac{1}{2}\,lgt + lg\left[U_{max}\cdot d\cdot\sqrt{\frac{D_e}{\pi}}\right], \quad (14)$$

where U_{max} – maximum amount of leached cobalt, mg/kg; d – matrix density, kg/m^3.

The leaching depth was calculated according to the following equation:

$$L_t^i = \sum_1^n\left(W_n^i\cdot\frac{t_n}{d}\right), \quad (15)$$

where L_t^i – leaching depth during time interval t_n, cm; d – sample density, g/cm^3.

The leaching index (L) was calculated as the decimal logarithm of the reciprocal of the effective diffusion coefficient:

$$L = lg\frac{1}{D_e}, \quad (16)$$

3. Results and discussion

3.1. Characterization of powder materials

3.1.1. Elemental composition and surface morphology by XRF and SEM-EDX

Solid waste from the production of boric acid (borogypsum) is a sludge with a high content of calcium Ca, silicon Si and, sulfur S (Table 1), which makes it expedient to use them as a raw material for obtaining solid calcium silicate matrices for the immobilization of cobalt radionuclides. During hydrothermal treatment, sulfur S is separated because of the formation of soluble sulfates, so its content in the resulting product is significantly reduced. The main components of the resulting product are Ca and Si, with the molar ratio Ca/Si = 1.1. The adsorbent samples contain an admixture of Fe at a low concentration of wt% = 5.75–6.41 % (Table 1).

Table 1
XRF elemental composition of boric acid waste, $CaSiO_3$ obtained from waste by hydrothermal method, and Co-saturated $CaCoSi_2O_6$.

Element	XRF composition of powder materials, wt%		
	Boric acid production waste	$CaSiO_3$, obtained from waste	$CaCoSi_2O_6$, saturated with Co^{2+}
Si	30.24	34.81	34.89
Ca	40.78	54.79	26.45
S	25.18	3.98	0.81
Fe	3.79	6.41	5.75
Co	0.00	0.00	32.10

SEM images of the surface of the initial calcium silicate, as well as the cobalt-saturated material, are presented in Fig. 2. The initial $CaSiO_3$ obtained by hydrothermal conversion of boric acid production waste has a pronounced layered structure, which is formed by elongated flat particles. The clearly distinguishable mesoporous structure of the sample, with a predominance of slit-like pores between long secondary particles, correlates with the shape of low-temperature nitrogen adsorption isotherms and density function theory (DFT) and Barrett-Joyner-Halend (BJH) pore size distributions (Fig. 5). Isotherms of low-temperature nitrogen adsorption on the initial adsorbent belong to type IV with an H3 hysteresis loop, which is typical for layered mesoporous solids. EDX mapping of $CaSiO_3$ obtained from boric acid production waste indicates a homogeneous phase composition due to the uniform distribution of the structural elements Si, Ca, and O over the surface of the material. The sample contains local inclusions of Fe with a relatively low mass concentration (up to 1.95 wt%).

After adsorption saturation of calcium silicate with cobalt ions, a significant change in the morphology of the material occurs, manifested in the formation of a microporous structure with an irregular pore shape. These changes are caused by the adsorption of Co^{2+} through the dissolution-precipitation mechanism in the slit-like pores of the original $CaSiO_3$ [45]. The powdery precursor of the ceramic matrix formed because of adsorption saturation for the immobilization of high-energy cobalt radionuclides has a 6-fold greater specific surface area (Fig. 5), which also coincides with the formation of many small $CaCoSi_2O_6$ agglomerates on the surface of the adsorbent (Fig. 2). According to the EDX mapping of the elemental distribution of Co over the surface of a saturated sample, the adsorption of Co^{2+} ions proceed uniformly, which indicates a uniform distribution of adsorption-active centers of calcium silicate.

3.1.2. Structural characterization by XRD and FTIR

XRD patterns of calcium silicate $CaSiO_3$ obtained from boric acid production wastes as well as cobalt-calcium silicate $CaCoSi_2O_6$ saturated with cobalt ions Co^{2+} are presented in (Fig. 3a). Both the original and cobalt-saturated samples have the most intense X-ray peak with a diffraction angle 2θ = 26.6°. Moreover, this diffraction maximum is retained after sintering of the ceramic matrices (Fig. 11b). In this regard, the samples are assumed to contain an impurity phase of quartz, SiO_2 (PDF #00-046-1045), that is also present in the borogypsum before hydrothermal treatment [47,48]. $CaSiO_3$ contains two crystalline modifications of calcium carbonate as side reaction products with atmospheric air: vaterite (PDF #00-033-0268) and calcite (PDF #00-005-0586). After the adsorption of cobalt, vaterite, which is unstable in an aqueous medium, turns into calcite [59]. The calcium silicate (wollastonite, $CaSiO_3$) and cobalt calcium silicate ($CaCoSi_2O_6$) phases crystallize only after sintering (Fig. 11b). Therefore, in powdered precursors of ceramic matrices, they are present in an amorphous form.

FTIR spectra of the initial calcium silicate obtained by hydrothermal conversion of boric acid production waste, as well as calcium silicate after saturation with cobalt ions Co^{2+}, are presented in Fig. 4. An intense absorption band with a wavenumber of 850–1100 cm^{-1} is associated with asymmetric vibrations of Si–O–Si cross-linking bonds, as well as with asymmetric and symmetric vibrations of Si—O terminal bonds [60–62]. The group of absorption bands in the region of 550–750 cm^{-1} is attributed to symmetrical vibrations of Si–O–Si cross-linking bonds in [SiO_4] tetrahedra. Absorption bands in the low-frequency region of 400–550 cm^{-1} are associated with deformation vibrations of terminal O–Si–O bonds and vibrations of calcium-oxygen bonds in [CaO_6] octahedra [63–65]. Absorption bands with wavenumbers of 1430 and 880 cm^{-1} are attributed to the calcium carbonate $CaCO_3$ [66–68]. The absorption bands in the regions of 1600 and 3400 cm^{-1} are caused by bending and stretching vibrations of crystallization water [60,65]. Indirect confirmation of a change in the structure of the samples because of adsorption saturation is the shift of the absorption band with a wave number of 972 cm^{-1} to the region of higher frequencies up to 1022

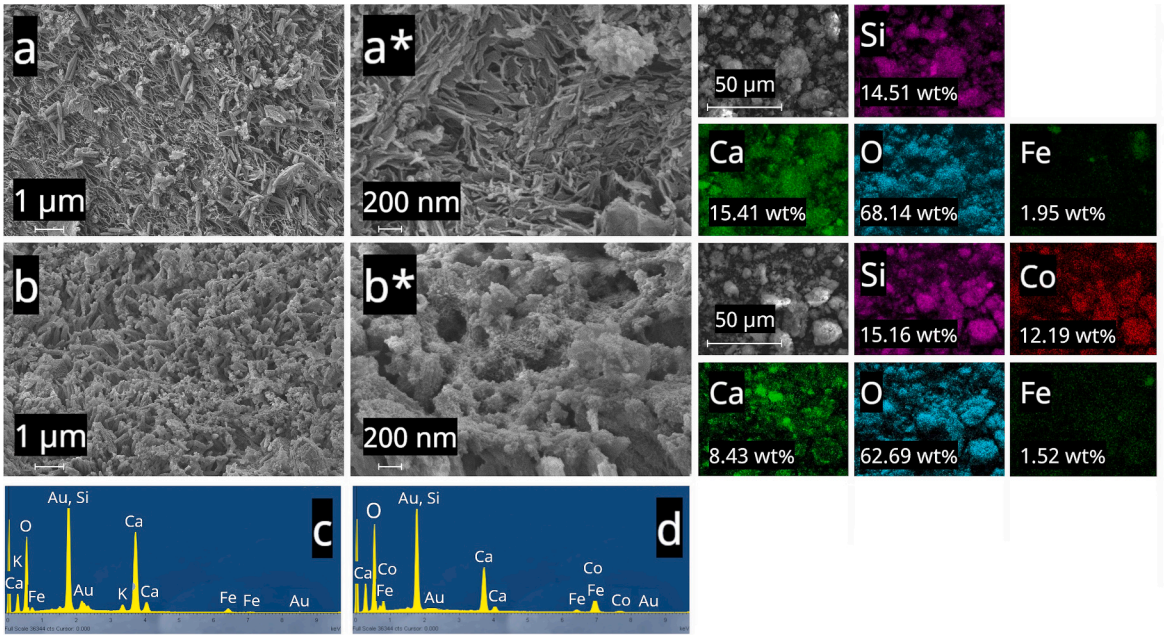

Fig. 2. SEM images and EDX spectra of (a, c) $CaSiO_3$, obtained from waste, and (b, d) Co-saturated $CaCoSi_2O_6$ powders.

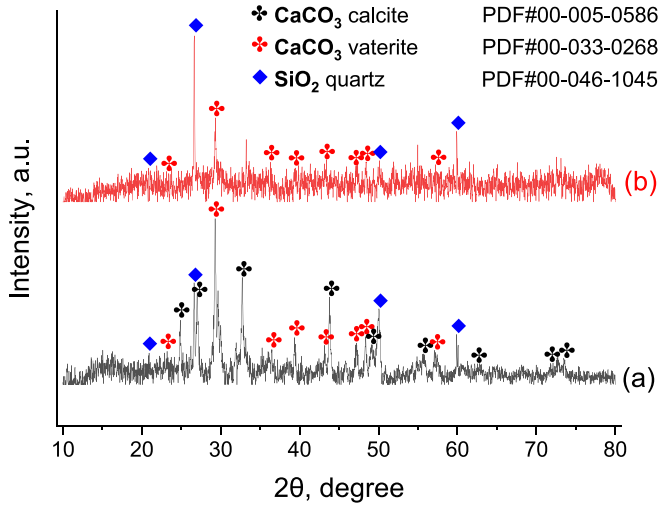

Fig. 3. XRD patterns of (a) $CaSiO_3$, obtained from waste, and (b) Co-saturated $CaCoSi_2O_6$.

cm^{-1}.

3.1.3. Porous characteristics and specific surface area study by low temperature gas (N_2, Ar) adsorption

The isotherm of low-temperature adsorption-desorption of nitrogen for the initial material $CaSiO_3$ obtained from waste products of boric acid production (Fig. 5) belongs to type IV according to the IUPAC classification, typical for mesoporous materials. The hysteresis loop for the initial material, $CaSiO_3$, belongs to the H3 type, which indicates the layered structure of the material and the slit-like shape of the pores. The pore size distribution obtained by the DFT method indicates the presence of meso- and macropores of various diameters from dp ≈ 5 nm to dp ≈ 75 nm without a clearly defined main pore diameter. The peaks of the pore size distribution curve obtained by the BJH method have a wide shape, which indicates the presence of a large range of pore diameters.

The specific surface area of the Co-saturated $CaCoSi_2O_6$ increases in 6 times (S_{BET} = 55.03 m^2/g for $CaSiO_3$, S_{BET} = 331.5 m^2/g for $CaCoSi_2O_6$). In this case, a significant change in the porous structure occurs, expressed in the disappearance of macropores, a decrease in the size of mesopores, and the appearance of many micropores. The main reason for the changes in pores structure is the adsorption of cobalt ions by the mechanism of dissolution-precipitation in the slit-like pores of the initial $CaSiO_3$ material [69]. As a result of cobalt adsorption, a network of channels is formed between $CaCoSi_2O_6$ particles, consisting of pores of smaller diameter. According to the DFT data, the porous structure of $CaCoSi_2O_6$ is represented by micropores with a diameter of dp ≈ 1 nm and mesopores with a size of dp ≈ 5 nm. According to the BJH data, the porous structure of saturated $CaCoSi_2O_6$ is represented by mesopores with a diameter of dp ≈ 2–5 nm. The shape of porous channels in $CaCoSi_2O_6$ is much more diverse than in $CaSiO_3$. That is confirmed by the change in the shape of the hysteresis loops to the hybrid type H2 + H3. Adsorption isotherms after adsorption saturation correspond to type IV, typical for mesoporous adsorbents, but with a much more significant contribution of micropores due to the appearance of a clearly defined initial vertical section.

For a detailed study of the structure of micropores, adsorption-desorption isotherms of Ar on the initial $CaSiO_3$ and saturated material $CaCoSi_2O_6$ (Fig. 6) were obtained. Since argon has a much smaller molecular size, it is preferable for determining the structure of micro- and mesopores. The adsorption-desorption isotherms of argon on the initial $CaSiO_3$ are of type I without a clearly defined hysteresis loop (Fig. 6a). The pore size distributions obtained by the HK and SF methods (Fig. 6c, e) indicate the presence of pores with diameters of dp = 0.42 nm and dp = 0.7 nm, respectively. The adsorption-desorption isotherms of argon on the saturated material $CaCoSi_2O_6$ also belong to type I and have a hysteresis loop of the hybrid type H2 + H3 (Fig. 6b), indicating a developed network of micropores. The pore size distributions obtained by the HK and SF methods (Fig. 6d, f) indicate the presence of pores with diameters of 0.4–0.5 nm and 0.8 nm, respectively.

3.1.4. Characterization of thermal transformations by TG/DTA

According to the thermogravimetric dependences of the thermogravimetric analysis (TG) and differential thermal analysis (DTA) (Fig. 7), heating the initial $CaSiO_3$ to 295 °C and the saturated $CaCoSi_2O_6$ material to 230 °C is accompanied by a decrease in mass with an endo effect on the differential thermal analysis curve associated with the evaporation of adsorbed water. When the temperature reaches 523 °C for the

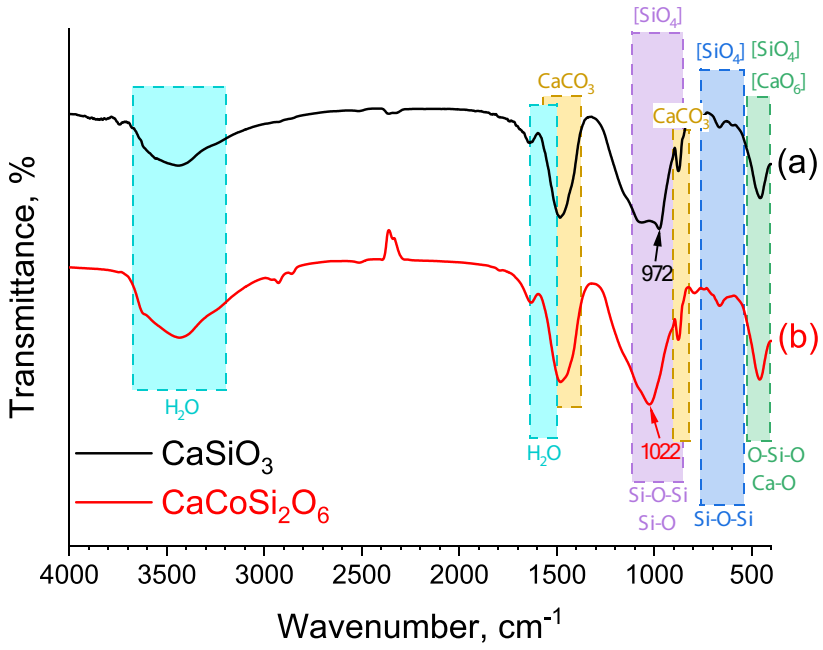

Fig. 4. FTIR spectra of (a) $CaSiO_3$, obtained from waste, and (b) Co-saturated $CaCoSi_2O_6$ powders.

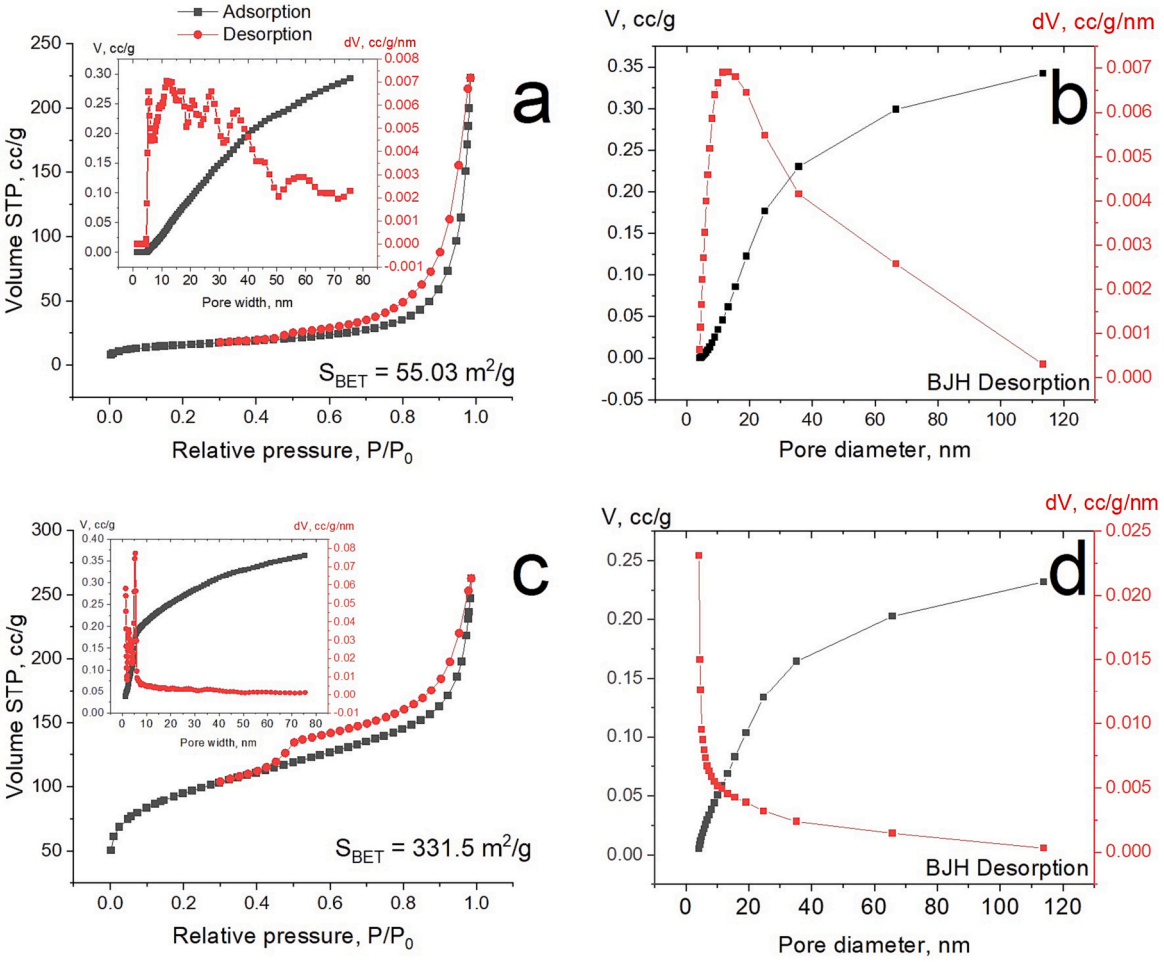

Fig. 5. Isotherms of low-temperature N_2 adsorption-desorption, DFT pore size distributions (a,c), and BJH desorption pore size distributions (b,d) of $CaSiO_3$ (a,b) and $CaCoSi_2O_6$ (c,d) obtained from waste.

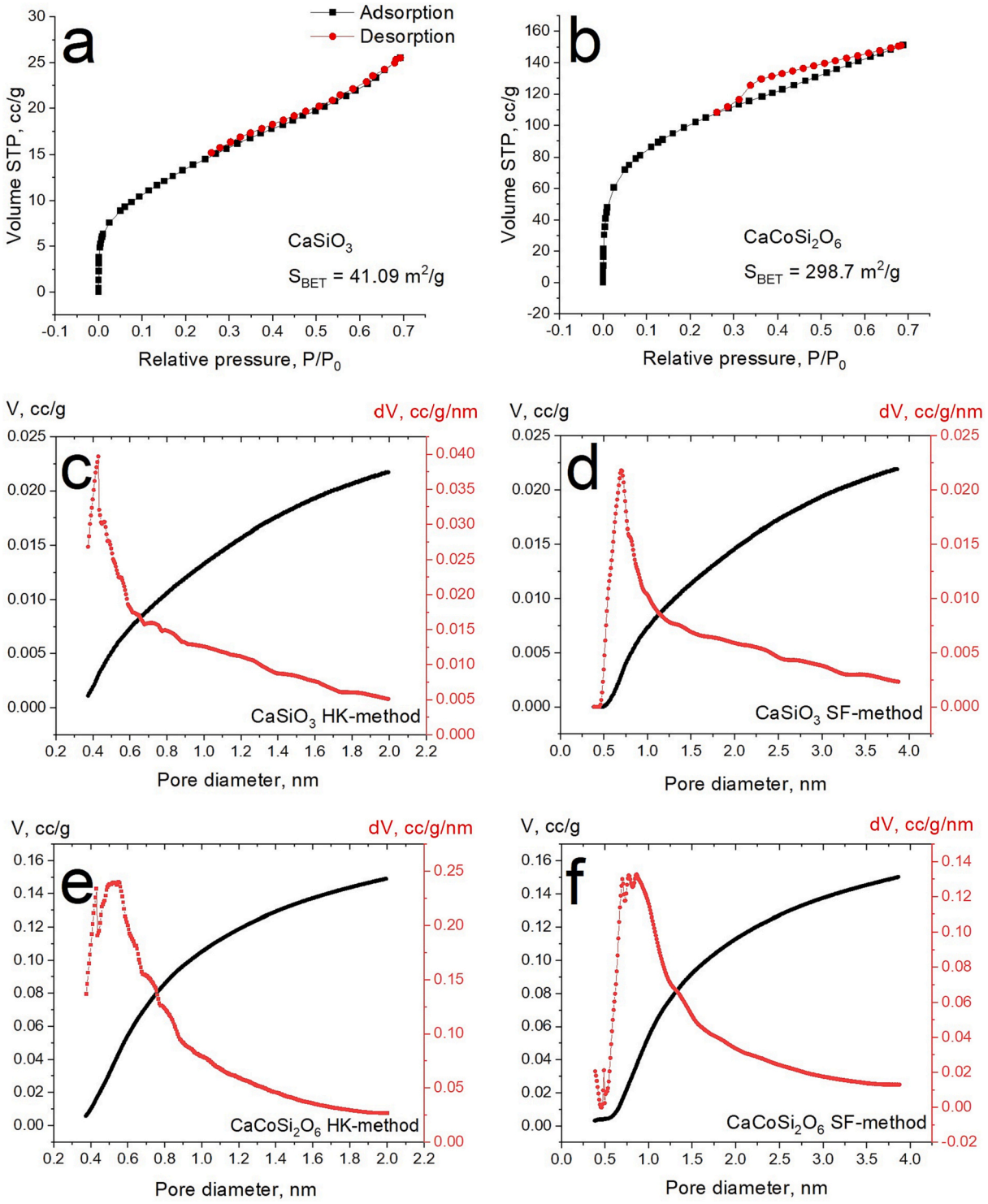

Fig. 6. Isotherms of low-temperature Ar adsorption-desorption for $CaSiO_3$ (a) and $CaCoSi_2O_6$ (b), HK and SF pore size distributions for $CaSiO_3$ (c, d) and $CaCoSi_2O_6$ (e, f).

original $CaSiO_3$ and 570 °C for the saturated $CaCoSi_2O_6$, mass loss begins with an endothermic effect caused by thermal decomposition of the $CaCO_3$ contained in the initial calcium silicate. After a temperature mark of 730–735 °C, the mass loss stops completely. The total mass loss for the initial $CaSiO_3$ is 20.5 %, and for the $CaCoSi_2O_6$, it is 18.2 %. A slight decrease in weight loss is associated with a smaller amount of adsorbed water in a saturated $CaCoSi_2O_6$ sample.

3.1.5. Granulometric composition

The granulometric composition of $CaCoSi_2O_6$ powder obtained from boric acid production waste and saturated with cobalt cations Co^{2+} (Fig. 8a) is represented by many fractions with particle sizes in a range of 0.1–60 μm. Large particles are formed by agglomerates of smaller ones with a spherical shape. The largest contribution to the granulometric composition of the material is made by fractions of an average size of 5–20 μm (≈47 %) and 1–5 μm (≈13 %), as well as a large fraction of 20–40 μm (≈32 %). The share of the finest fraction <1 μm accounts for

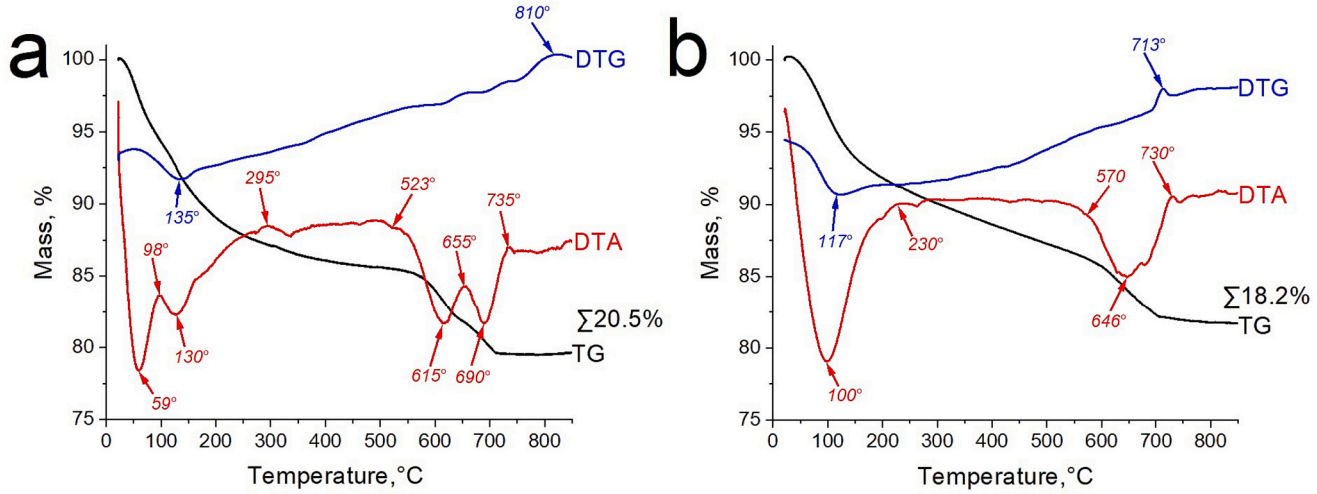

Fig. 7. TG, TGA and DTA curves of initial $CaSiO_3$ (a) and Co-saturated $CaCoSi_2O_6$ (b) powders.

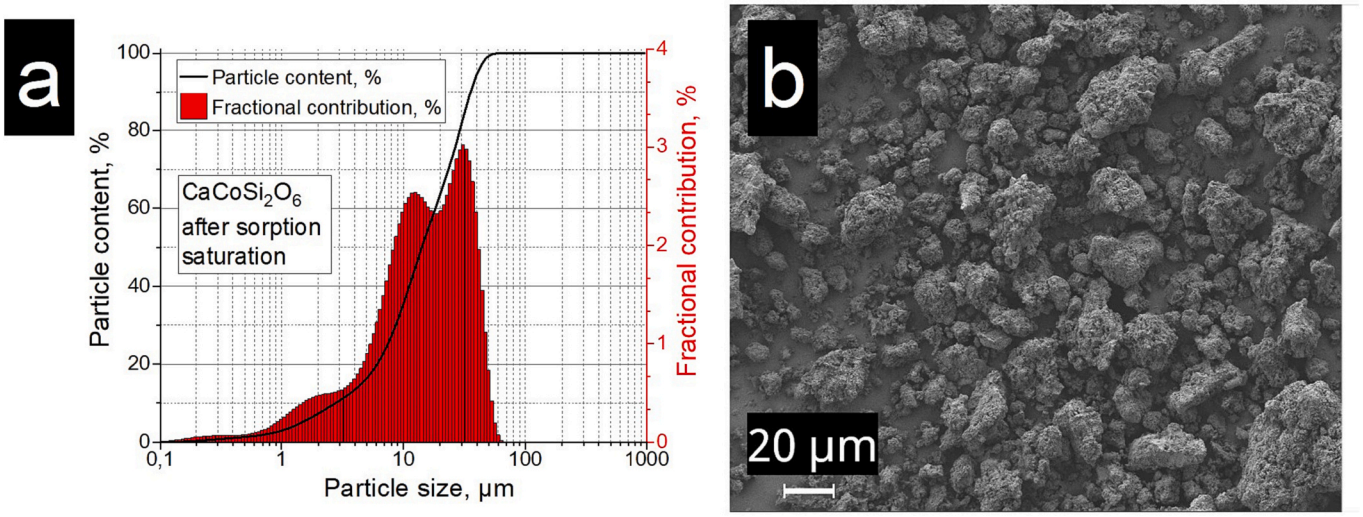

Fig. 8. Particle size distribution (a) and SEM image (b) of saturated $CaCoSi_2O_6$ powder.

≈3 % of the total number of particles, and the largest fraction 40–60 μm is ≈5 % of the particles. Thus, ≈79 % of the $CaCoSi_2O_6$ powder particles are 5–40 μm in size, which is also confirmed by SEM images of the material (Fig. 8b). The presence of a wide range of fractions with different particle sizes has a positive effect on the key physical properties of ceramics (strength, hardness, and hydrolytic stability) obtained from powder materials and facilitates the sintering process.

3.2. Study of Co^{2+} ions adsorption on $CaSiO_3$

3.2.1. Equilibrium adsorption study

Adsorption isotherms of Co^{2+} ions on calcium silicate synthesized from boric acid production waste are shown in (Fig. 9a). The adsorption isotherms refer to the H-type according to the Giles classification, which indicates the ion-exchange nature of Co^{2+} adsorption. The presence of an initial vertical section characterizes the high affinity of the adsorbate for the adsorbent in the region of low concentrations. The dependence of the solution purification efficiency on the initial concentration of cobalt ions (Fig. 9b) shows that a high degree of purification (R > 99 %) is retained if the initial concentration $C(Co^{2+})$ is lower than 35 mmol/l.

The values of the coefficients of the Freundlich, Langmuir, and Langmuir-Freundlich isotherm models are presented in (Table 2). The values of the coefficient of determination R^2 for the Langmuir isotherm ($R^2 = 0.931$) are lower than for the Freundlich isotherms ($R^2 = 0.980$) and Langmuir-Freundlich isotherms ($R^2 = 0.990$). An additional power coefficient n in the Langmuir-Freundlich equation significantly increases the determination coefficient (up to $R^2 = 0.99$). The Langmuir-Freundlich equation is also characterized by the lowest value of the Pearson criterion $\chi^2 = 0.037$ and other error functions: SSE = 0.149, MSE = 0.021, and HYBRID = 11.471. The combination of the values of the compliance criteria R^2, χ^2, SSE, MSE, and HYBRID indicates that the Langmuir-Freundlich model most accurately describes the experimental data. The Freundlich model is the second best in terms of the degree of agreement between the predicted values and the experimental ones. The Langmuir model has low values of the coefficient of determination $R^2 = 0.931$, as well as high values of other criteria: $\chi^2 = 0.197$, SSE = 0.983, MSE = 0.140, and HYBRID = 23.957. The Langmuir model has low values of the coefficient of determination $R^2 = 0.931$, as well as high values of other criteria: $\chi^2 = 0.197$, SSE = 0.983, MSE = 0.140, and HYBRID = 23.957, therefore, this model does not accurately describe the real data of Co^{2+} adsorption from solution. However, to assess the comparative evaluation of the adsorption capacity of the material, we used the experimental value of the adsorption capacity $Q_{max} = 3.742$ mmol/g, because the adsorption capacity $Q_{LF} = 5.657 \pm 1.826$ mmol/g predicted by the Langmuir-Freundlich equation was not achieved in the studied concentration range.

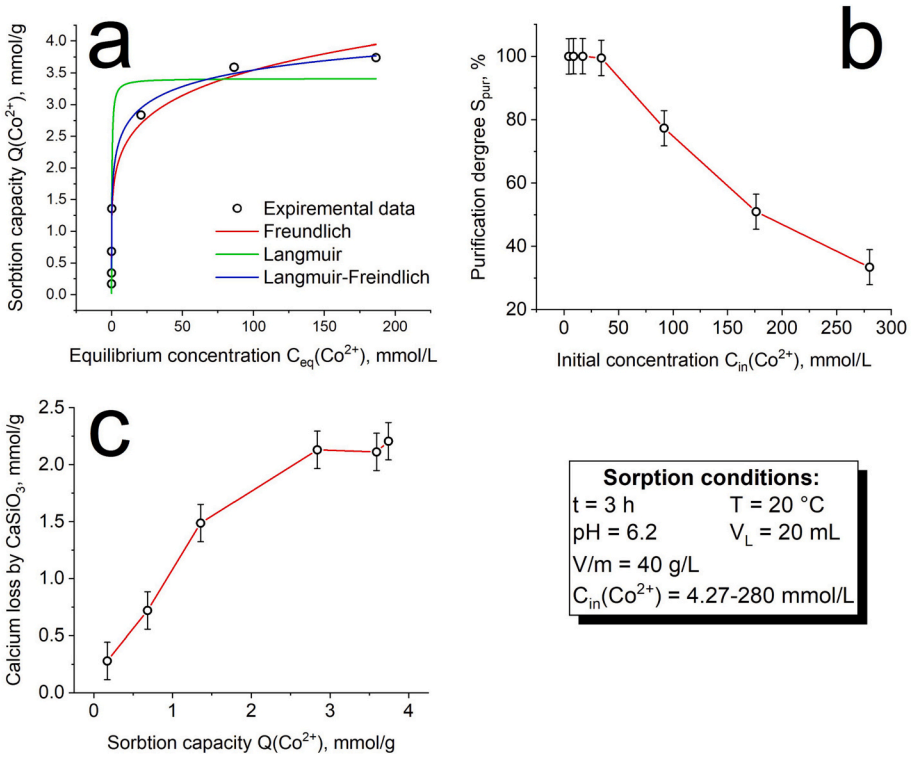

Fig. 9. (a) Isotherm of Co^{2+} adsorption on $CaSiO_3$, (b) – removal efficiency with various initial of Co^{2+} concentrations (c) – Ca^{2+} leaching by $CaSiO_3$ as a plot of adsorption capacity.

Table 2
Equilibrium parameters for the adsorption of Co^{2+} on $CaSiO_3$ obtained from waste.

Parameters	Isotherm model			Experimental data
	Freundlich	Langmuir	Langmuir-Freundlich	
Q_{max}, mmol/g	–	3.413 ± 0.260	5.657 ± 1.826	3.742
K, L/mmol	1.596 ± 0.133	3.658 ± 2.051	0.467 ± 0.273	–
n	0.173 ± 0.018	–	0.278 ± 0.063	–
R^2	0.980	0.931	0.990	–
χ^2	0.057	0.197	0.037	–
SSE	0.287	0.983	0.149	–
MSE	0.041	0.140	0.021	–
HYBRID	18.405	23.957	11.471	–

3.2.2. Proposed adsorption mechanism

After reaching the value of the adsorption capacity of 3 mmol(Co^{2+})/g, there was a noticeable deviation in the dependence of the specific loss of calcium ions, mmol(Ca^{2+})/g as a function of the adsorption capacity for cobalt, mmol(Co^{2+})/g from direct proportionality (Fig. 9b). Thus, the adsorption of Co^{2+} ions on calcium silicate obtained from waste products of boric acid proceeded in two clearly distinguishable stages: (1) adsorption to 3 mmol(Co^{2+})/g is mainly due to ion exchange, (2) further adsorption after 3 mmol(Co^{2+})/g is due to other mechanisms mainly by surface complexation of an intra- and innerspheric interaction occurring between hydrated cobalt ions and active >Si-OH and >Ca-OH groups [23–26]. A schematic representation of the proposed adsorption mechanism and the stages of Co^{2+} ions adsorption is shown in Fig. 10.

3.2.3. Adsorption capacity comparison

The adsorption capacity was compared with similar adsorption materials for the extraction of Co^{2+} obtained from secondary resources (Table 3). The adsorption capacity for Co^{2+} ions of 220.7 mg/g for calcium silicate obtained from boric acid production waste exceeds the capacity values for most similar materials. It should be noted that the value of the adsorption exchange capacity for $CaSiO_3$ synthesized from boric acid production wastes practically coincides with the value of adsorption capacity of model $CaSiO_3$ of 195.7 mg/g [41].

3.3. Characterization of $CaCoSi_2O_6$ solid-state matrices obtained by SPS

3.3.1. SPS consolidation kinetics and phase composition

According to the dilatometric shrinkage rate curves of the $CaCoSi_2O_6$ specimens obtained by the SPS method at different temperatures of 800 °C, 900 °C, and 1000 °C (Fig. 11a), material sintering occurs in two stages. The course of stage I is observed in the first 2 min of the sintering process, up to a temperature of 600–700 °C. As a result of mechanical action during powder pressing and subsequent deformation, destruction, rearrangement, and compaction of $CaCoSi_2O_6$ particles, the shrinkage rate during stage I changes in the range of 9.7–10.6 mm/min. Stage II, associated with thermal action on powder particles, is the main stage of the sintering process, during which the final consolidation of the material into solid ceramic matrices occurs due to the diffusion of plastic deformation and viscous flow of the material. Consolidation of $CaCoSi_2O_6$ is completed at a temperature of 900 °C, as can be seen from the dilatometric shrinkage rate curves (Fig. 11a). Therefore, for the sample obtained at a temperature of 800 °C, stage II was not observed, and the sintering of the material was not completed. For the sample sintered at a temperature of 900 °C, the shrinkage rate during stage II was 0.8 mm/min, and for the sample obtained at a temperature of 1000 °C, it was 2.2 mm/min. Stage II proceeded for 2–3 min, after which further shrinkage ceased.

XRD patterns of samples of $CaCoSi_2O_6$ ceramic matrices obtained by the SPS method at various temperatures of 800 °C, 900 °C, 1000 °C (Fig. 11b) and of the initial $CaCoSi_2O_6$ powder are shown in (Fig. 11b). The phase composition of the materials is represented by the crystalline phases of the initial calcium silicate $CaSiO_3$ of wollastonite crystalline

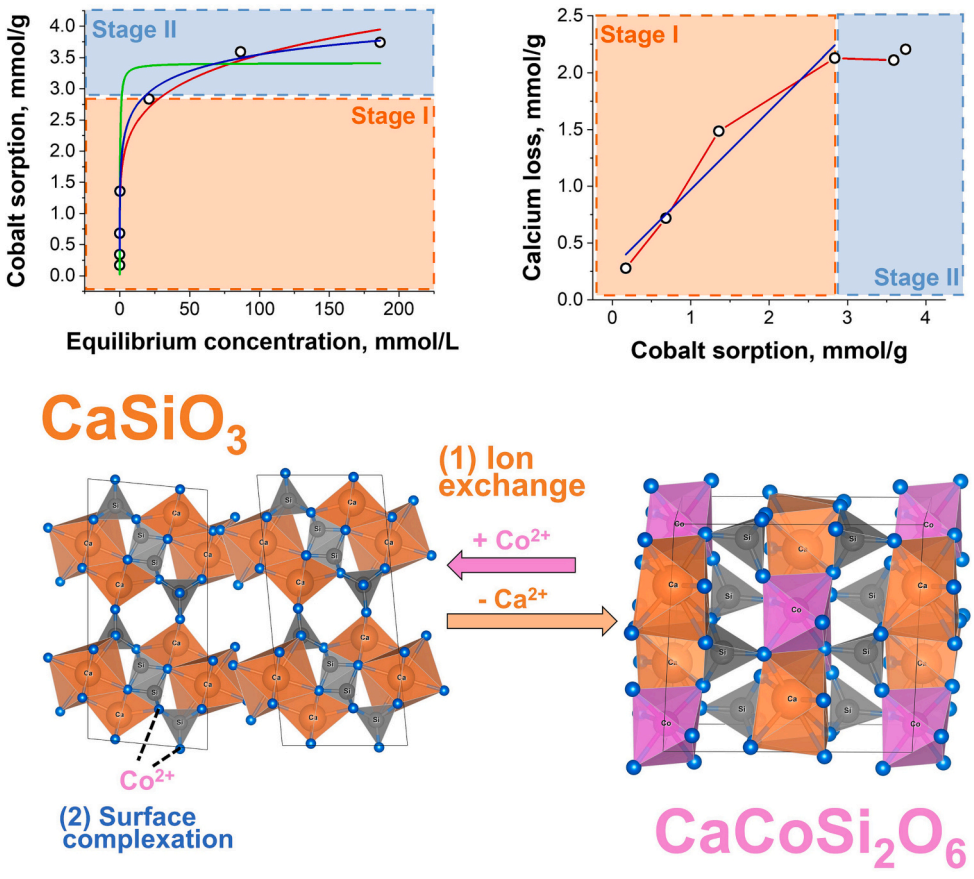

Fig. 10. Proposed cobalt ions Co^{2+} adsorption mechanism on calcium silicate obtained from boric acid production waste.

Table 3
Comparative characteristics of adsorbents for Co^{2+} obtained from industrial waste.

Adsorbent	Adsorption capacity q, mg/g	Specific surface, m^2/g	Experimental conditions				
			C(Co^{2+})	V/m, ml/g	t, °C	Time, h	pH
Biochar from mustard waste biomass [70]	24	354.07	12–240 mg/l	1:125	25	24	5.0
Zeolitic material from fly ash [71]	37.13	9.24	100–6000 μmol/l	1:400	22	6	6.0
Chitosan modified biochar from agricultural waste [72]	27.38	134	50–600 mg/l	1:200	–	20	5.0
Mesoporous calcium silicate from coal fly ash [73]	154.8	–	500 mg/l	1:500	25	4	2–7
11 Å tobermorite from the remnants of the disposal of newsprints [74]	10.47	–	100 mg/l	1:20	20	1–120 min	1.0
Cancrinite-type zeolite from fly ash [75]	73.3	278.9	0.5–4 mmol/l	1:2000	25	72	6.0
Chemically modified waste almond green hull [76]	45.5	–	18–110 mg/l	3–8 mg/l	15–35	< 7 min	–
Hydroxyapatite from eggshell waste [77]	457	–	50–500 mg/l	–	25	80 min	–
Calcium silicate (model) [41]	195.7	55.8	4.27–280 mmol/l	1:40	20	24	–
Calcium silicate from boric acid production waste [this work]	220.8	55.03	4.27–280 mmol/l	1:40	20	3	–

modification with monoclinic syngony (PDF #00-029-0372) and the calcium-cobalt silicate $CaCoSi_2O_6$ (PDF #00-084-1288) formed because of ion exchange. In addition, there is an impurity phase of quartz, SiO_2 (PDF #00-046-1045). As a result of sintering, the complete decomposition of the calcium carbonate contained in the original powder occurs. The phase of monoclinic $CaCoSi_2O_6$ is extremely stable and does not dissolve in water and organic solvents [78].

3.3.2. *Ceramic matrices morphology and elemental composition by SEM-EDX*

The surface morphology of the $CaCoSi_2O_6$ sample obtained by SPS at 800 °C from boric acid waste (Fig. 12b, b*) confirms that sintering was not completed at this temperature. The surface of the material is not monolithic and has clearly defined pores, as well as inclusions of agglomerates of particles of the original powder. As the sintering temperature rises to 900 °C, particles of the initial $CaCoSi_2O_6$ powder consolidate into a dense ceramic matrix, and the sample surface becomes uniform (Fig. 12c). However, a small number of microdefects, pores, and agglomerates of the initial particles are observed (Fig. 12c*). With a further increase in the SPS temperature to 1000 °C, the surface of the solid matrix is almost completely devoid of structural defects due to the intensification of the sintering process (Fig. 12d, d*). The elemental composition of the $CaCoSi_2O_6$ material obtained from boric acid production waste is close to the composition of the model $CaCoSi_2O_6$ [41],

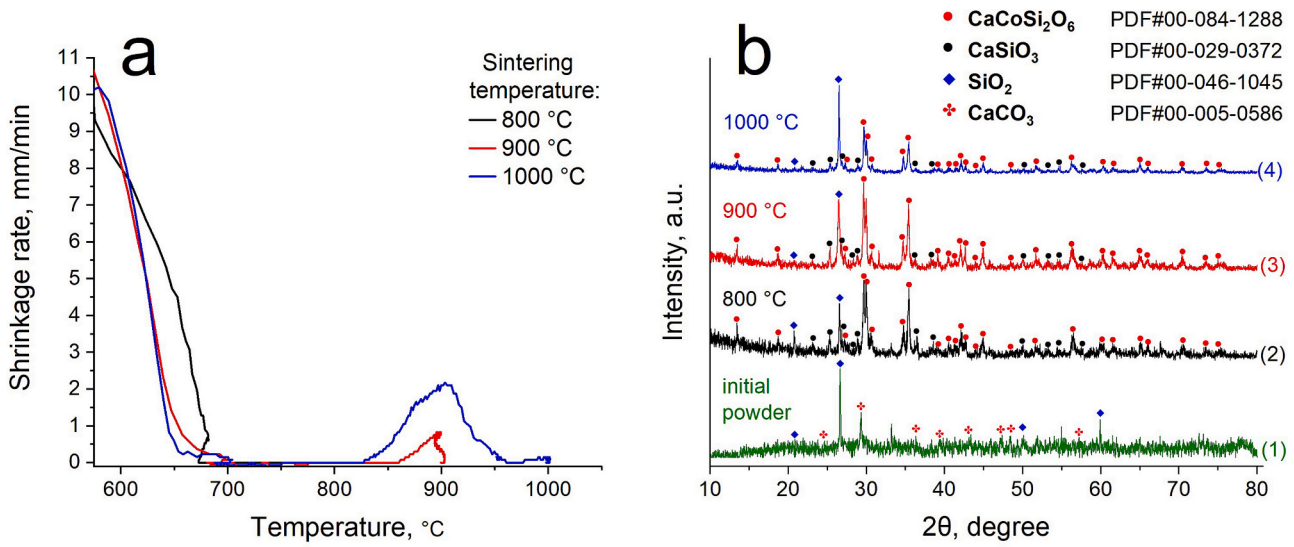

Fig. 11. Shrinkage rates (a) and X-ray diffractograms (b) of initial $CaCoSi_2O_6$ powders (1) and solid-state matrices, obtained by SPS at a temperature of 800 °C (2), 900 °C (3) and 1000 °C (4).

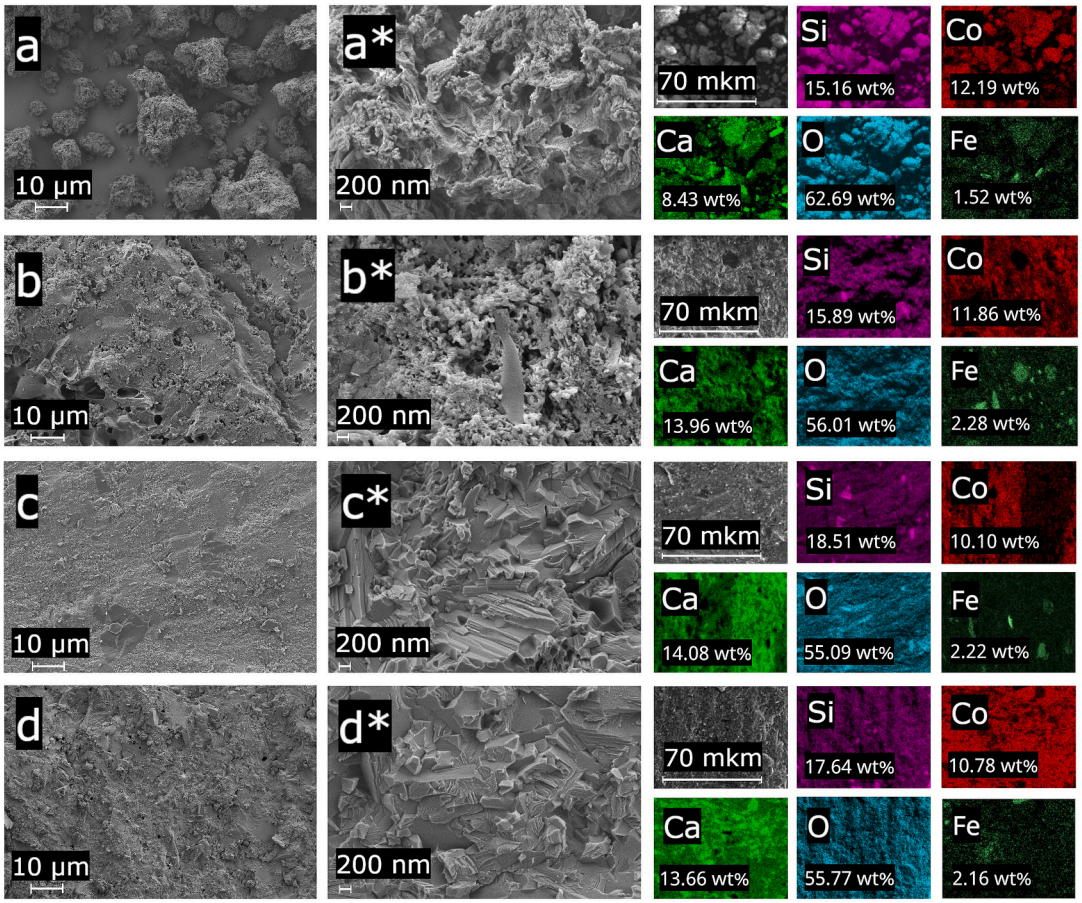

Fig. 12. SEM images and EDX mapping of $CaCoSi_2O_6$ initial powder (a and a*) and ceramic matrices obtained by SPS at various temperatures: 800 °C (b and b*), 900 °C (c and c*), 1000 °C (d and d*).

except for the presence of an iron impurity (w(Fe) < 2.3 wt%). In places where iron atoms are concentrated on the maps of the distribution of elements (Fig. 12), defects in the structure of the matrix surface (pores and violations of the monolithic structure) are visible, therefore, to improve the quality of ceramics, it is necessary to further clean the raw materials for synthesis from iron impurities.

3.3.3. *Microhardness characterization*

Diagrams of microhardness of $CaCoSi_2O_6$ samples obtained by SPS at different temperatures (Fig. 13) demonstrate the non-linear nature of

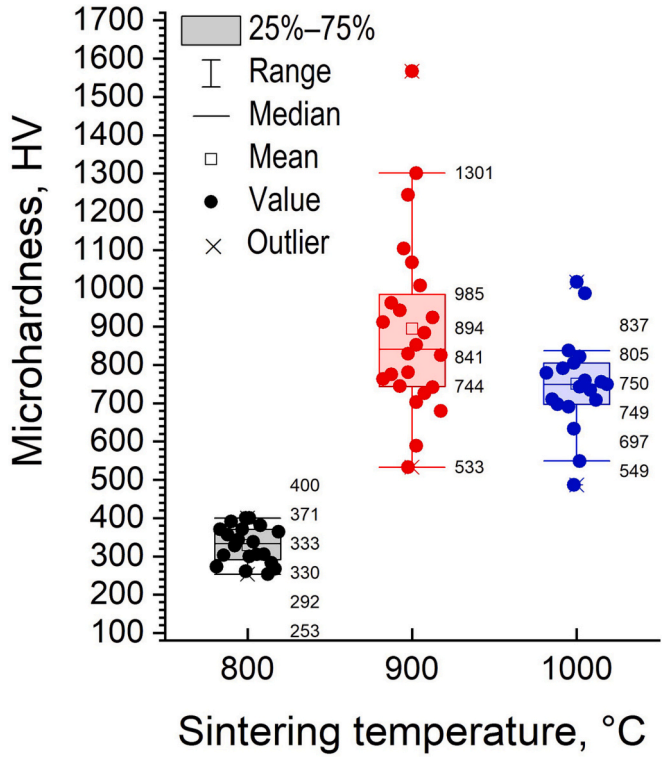

Fig. 13. Vickers microhardness of $CaCoSi_2O_6$ obtained by SPS at 800 °C, 900 °C and 1000 °C.

the change in this parameter with increasing sintering temperature. For a sample sintered at 900 °C, the microhardness varies in the range of 744–985 HV, and the average microhardness is 894 HV, which is the highest value of this indicator in the range of the studied sintering temperatures. However, the measurement results for this sample have the highest dispersion and statistical asymmetry, which indicates the structural inhomogeneity of the ceramic matrix. The presence of measurement results with values >1300 HV indicates the local formation of extremely hard grains and grain agglomerates in the ceramic matrix. During sintering at a temperature of 1000 °C, the microhardness changes in the range of 697–805 HV, and the average value of the microhardness is 760 HV. The set of measurement results has less statistical heterogeneity. The absence of microhardness values well above 1000 HV indicates more uniform compaction than at 900 °C.

3.3.4. *Hydrolytic stability*

The $CaCoSi_2O_6$ ceramic matrices obtained by SPS at 1000 °C has the lowest Co^{2+} ion leaching rate (Fig. 14a). The leaching rate on the 30th day for this sample (1000 °C) was 2.04×10^7 g/cm^2/day^1, which meets the requirements established by GOST R 52126-2003 (ISO 6961:1982) for highly active waste. The slope of the straight line Lg(Bt) vs lg t for all obtained samples lies in the range from 0.5 to 1 (Fig. 14b), which, according to the de Groot and der Slot model, indicates a complex leaching mechanism due to diffusion and dissolution of the matrix surface, while the dissolution of the matrix surface occurs earlier than diffusion through its dense structure. The leaching depth for the $CaCoSi_2O_6$ sample produced by the SPS method at 800 °C is significantly higher than for the $CaCoSi_2O_6$ samples obtained at 900 °C and 1000 °C (Fig. 14c), indicating that no final formation occurs at this sintering temperature. Solid ceramic matrix and is in good agreement with SEM data and matrix consolidation kinetics at SPS. The sample obtained by

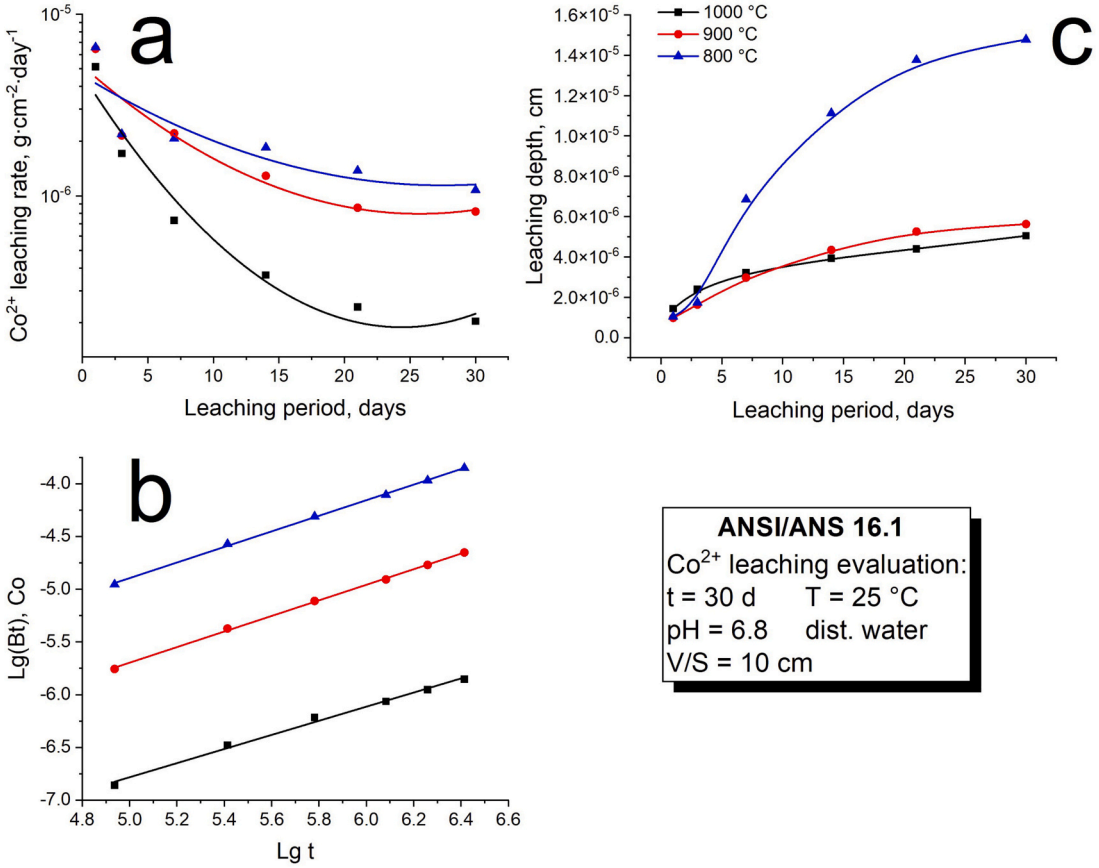

Fig. 14. Leaching rate of Co^{2+} ions (a), plots of lg(Bt) vs lgt (b) and leaching depth vs t (c) for matrices obtained by SPS at 800 °C, 900 °C and 1000 °C.

the SPS method at a temperature of 1000 °C also has the lowest diffusion coefficient of 1.07×10^{-12} and the highest value of the leaching index of 11.81 (Table 4).

3.3.5. Physical and mechanical properties

The compressive strength values (Table 5) for all obtained samples exceed the standard set by GOST R 52126-2003 of 9 MPa. With an increase in the sintering temperature, the physical and mechanical characteristics of ceramic matrices increase significantly (Table 5) due to their final consolidation, the disappearance of pores, and structural defects. The compressive strength increases by 2.5 times with an increase in the SPS temperature from 800 °C to 1000 °C.

The density of ceramic matrices increases by 15 % with an increase in the sintering temperature to 1000 °C (Table 5). Due to uneven compaction, the value of microhardness for a sample sintered at 900 °C is 8.34 GPa, which is 10 % higher than for a sample obtained at 1000 °C. At the same time, the remaining physical and mechanical characteristics (Table 5), leaching parameters (Table 4) and uniformity of surface morphology (Fig. 12), allow us to conclude that sintering at a temperature of 1000° is optimal.

4. Conclusions

Mesoporous calcium silicate was obtained by hydrothermal synthesis in an alkaline environment of waste products of boric acid (borogypsum). Using FTIR, XRF and EDX, N_2 adsorption-desorption methods, it was shown that the obtained material consisted of amorphous calcium silicate with an admixture of calcium carbonate, had a specific surface area of 55.0 m^2/g with a predominant pore size in the range of 5–75 nm. The adsorbent obtained from borogypsum waste was characterized by a higher cobalt adsorption capacity of 220.8 mg/g in comparison with analogues. Cobalt adsorption proceeded mainly due to ion exchange and led to the formation of a phase of mixed calcium silicate-cobalt $CaCoSi_2O_6$. Sintering of Co-saturated adsorbents in $CaCoSi_2O_6$ ceramic matrices was performed by the SPS method at a temperature of 800–1000 °C. The samples obtained at 1000 °C had a defect-free structure and the highest physico-chemical characteristics (compressive strength up to 481 MPa, microhardness up to 7.54 GPa, cobalt leaching rate $< 2.04 \times 10$–7 g/($cm^2 \times$ day), the leaching index of 11.81, and the leaching depth $< 5.04 \times 10^6$ cm) that complied with the requirements for solid radioactive waste in GOST R 52126-2003, ANSI/ANS 16, and ISO 6961:1982. $CaSiO_3$ material has the prospects for further industrial applications, as well as reduces anthropogenic pollution through the use of dump borogypsum.

CRediT authorship contribution statement

O.O. Shichalin: Investigation, Writing – review & editing. **S.B. Yarusova:** Conceptualization, Methodology, Writing – original draft. **N. P. Ivanov:** Formal analysis, Investigation. **E.K. Papynov:** Investigation, Project administration, Resources. **A.A. Belov:** Investigation. **S.A. Azon:** Investigation. **I.Yu Buravlev:** Data curation, Visualization. **A.V. Myagchilov:** Investigation. **A.N. Fedorets:** Investigation, Validation. **V. L. Rastorguev:** Investigation, Validation. **Ya.G. Zernov:** Investigation, Validation. **S.Yu. Budnitskiy:** Investigation. **V.Yu Mayorov:** Investigation. **E.A. Gridasova:** Investigation, Validation. **I.G. Tananaev:** Formal analysis, Validation. **A.I. Ivanets:** Formal analysis, Validation, Writing – review & editing. **P.S. Gordienko:** Conceptualization, Data curation, Formal analysis.

Declaration of competing interest

The authors declare that they have no known competing financial interests or personal relationships that could have appeared to influence the work reported in this paper.

Table 4
Parameters of Co^{2+} leaching from $CaCoSi_2O_6$ matrices in 30 days.

Sintering temperature, °C	Diffusion coefficient, cm^2/s	Leaching rate for Co^{2+}, g/($cm^2 \times$ day)	Leaching index	Leaching depth, cm
1000	1.07×10^{-12}	2.04×10^{-7}	11.81	5.04×10^{-6}
900	4.85×10^{-11}	8.19×10^{-7}	10.31	5.63×10^{-6}
800	2.50×10^{-10}	1.08×10^{-6}	9.60	1.48×10^{-5}

Table 5
Physical and mechanical properties of $CaCoSi_2O_6$ matrices obtained by SPS.

Sintering temperature, °C	Density, g/cm^3	Compressive strength, MPa	Microhardness, GPa
800	2.89	193	3.29
900	3.25	429	8.34
1000	3.33	481	7.54

Data availability

Data will be made available on request.

Acknowledgments

The study was financial supported within the State Assignment of the Ministry of Science and Higher Education of the Russian Federation, topic No. FZNS-2023-0003. The work involved equipment of integrated common use center and interdisciplinary in the field of nanotechnologies and new functional materials (Far Eastern Federal University, Vladivostok, Russia).

References

[1] M.A. Islam, D.W. Morton, B.B. Johnson, B.K. Pramanik, B. Mainali, M.J. Angove, Opportunities and constraints of using the innovative adsorbents for the removal of cobalt(II) from wastewater: a review, Environ. Nanotechnol. Monit. Manag. 10 (2018) 435–456, https://doi.org/10.1016/j.enmm.2018.10.003.
[2] M. Araissi, E. Elaloui, Y. Moussaou, The removal of cadmium, cobalt, and nickel by adsorption with Na-Y zeolite, Iran. J. Chem. Chem. Eng. 39 (2020) 169–179, https://doi.org/10.30492/ijcce.2018.32096.
[3] A. Ivanets, I. Shashkova, N. Kitikova, A. Dzikaya, N. Nekrasova, V. Milyutin, O. Baigenzhenov, K. Zaruba-Venhlinskaya, A. Radkevich, Composite metal phosphates for selective adsorption and immobilization of cesium, strontium, and cobalt radionuclides in ceramic matrices, J. Clean. Prod. 376 (2022) 134104, https://doi.org/10.1016/j.jclepro.2022.134104.
[4] F. Hossain, Natural and anthropogenic radionuclides in water and wastewater: sources, treatments and recoveries, J. Environ. Radioact. 225 (2020), https://doi.org/10.1016/j.jenvrad.2020.106423.
[5] S. Yefremova, A. Kablanbekov, B. Satbaev, A. Zharmenov, Rice husk-based adsorbents for removal of metals from aqueous solutions, Materials 16 (2023), https://doi.org/10.3390/ma16237353.
[6] H. Moukadiri, H. Noukrati, H. Ben Youcef, I. Iraola, V. Trabadelo, A. Oukarroum, G. Malka, A. Barroug, Impact and toxicity of heavy metals on human health and latest trends in removal process from aquatic media, Int. J. Environ. Sci. Technol. (2023), https://doi.org/10.1007/s13762-023-05275-z.
[7] S. Kainth, P. Sharma, O.P. Pandey, Green sorbents from agricultural wastes: a review of sustainable adsorption materials, Appl. Surf. Sci. Adv. 19 (2024) 100562, https://doi.org/10.1016/j.apsadv.2023.100562.
[8] D. Bulgariu, L. Nemeş, I. Ahmad, L. Bulgariu, Isotherm and kinetic study of metal ions sorption on mustard waste biomass functionalized with polymeric thiocarbamate, Polymers (Basel) 15 (2023), https://doi.org/10.3390/polym15102301.
[9] N. Mudruk, M. Maslova, The effect of sorbent composition on sorption properties of materials based on Ti-Ca-Mg phosphates, Int. J. Mol. Sci. 24 (2023), https://doi.org/10.3390/ijms24097903.
[10] P.A. Nishad, A. Ajaykumar, A. Bhaskarapillai, Enhancing the metal ion binding characteristics and reversal of selectivity of crosslinked chitosan sorbents through functionalisation for targeted applications, Int. J. Biol. Macromol. 246 (2023), https://doi.org/10.1016/j.ijbiomac.2023.125720.
[11] M. Motlochová, L. Szatmáry, E. Pližingrová, P. Salačová, R. Fajgar, S. Lidin, J. Šubrt, Highly efficient eco-friendly sodium titanate sorbents of Cs(i), Sr(ii), Co

(ii) and Eu(iii): synthesis, characterization and detailed adsorption study, RSC Adv. 14 (2024) 743–754, https://doi.org/10.1039/d3ra05663e.
[12] T.S. Ngo, C.T. Tracey, A.G. Navrotskaya, A.V. Bukhtiyarov, P.V. Krivoshapkin, E. F. Krivoshapkina, Reusable carbon dot/chitin nanocrystal hybrid sorbent for the selective detection and removal of Cr(VI) and Co(II) ions from wastewater, Carbohydr. Polym. 304 (2023), https://doi.org/10.1016/j.carbpol.2022.120471.
[13] A.S. Saleh, A.G. Ibrahim, E.M. Elsharma, E. Metwally, T. Siyam, Radiation grafting of acrylamide and maleic acid on chitosan and effective application for removal of Co(II) from aqueous solutions, Radiat. Phys. Chem. 144 (2018) 116–124, https://doi.org/10.1016/j.radphyschem.2017.11.018.
[14] D. Smržová, L. Szatmáry, P. Ecorchard, A. Machálková, M. Maříková, P. Salačová, M. Straka, Carbon and zeolite-based composites for radionuclide and heavy metal sorption, Heliyon 8 (2022) e12293, https://doi.org/10.1016/j.heliyon.2022.e12293.
[15] S. Jain, N. Banthia, T. Troczynski, Conditioning of simulated cesium radionuclides in NaOH-activated fly ash-based geopolymers, J. Clean. Prod. 380 (2022) 134984, https://doi.org/10.1016/j.jclepro.2022.134984.
[16] L. Aloui, S. Mezghich, L. Mansour, S. Hraiech, F. Ayari, Swift removal of the heavy metals cadmium and Lead from an aqueous solution by a CAN-zeolite synthesized from natural clay, ChemEngineering 7 (2023) 113, https://doi.org/10.3390/chemengineering7060113.
[17] J. Du, J. Sun, D. Zhang, Preparation of modified zeolite/chitosan composites and study on the adsorption performance of Pb^{2+}, Polym. Eng. Sci. 64 (2024) 196–206, https://doi.org/10.1002/pen.26539.
[18] Y. Dehmani, B. Ba Mohammed, R. Oukhrib, A. Dehbi, T. Lamhasni, Y. Brahmi, A. El-Kordy, D.S.P. Franco, J. Georgin, E.C. Lima, A.A. Alrashdi, N. Tijani, S. Abouarnadasse, Adsorption of various inorganic and organic pollutants by natural and synthetic zeolites: a critical review, Arab. J. Chem. 17 (2024) 105474, https://doi.org/10.1016/j.arabjc.2023.105474.
[19] S.K. G.V., C.S. Matli, Synthesis and characterisation of pure zeolite A from fly ash for removal of lead and cadmium, Int. J. Environ. Anal. Chem. (2024) 1–23, https://doi.org/10.1080/03067319.2024.2301928.
[20] I. Dianellou, F. Karantoumanis, P. Tsamos, F. Noli, The effect of irradiation on the Cs, Co and Eu-removal from aqueous solutions using Greek minerals, J. Radioanal. Nucl. Chem. 332 (2023) 1923–1933, https://doi.org/10.1007/s10967-023-08857-w.
[21] M.V. Kravchenko, O.A. Diyuk, I.Z. Zhuravlev, S.I. Meleshevych, I.V. Romanova, Impact of hydrothermal treatment on the porous structure and adsorption properties of spherically granulated zirconium silicate, J. Inorg. Organomet. Polym. Mater. 33 (2023) 2346–2353, https://doi.org/10.1007/s10904-023-02663-3.
[22] M.R. Abass, R.A. Abou-Lilah, M.M. Abou-Mesalam, Selective separation of cobalt ions from some fission products using synthesized inorganic sorbent, J. Inorg. Organomet. Polym. Mater. (2024), https://doi.org/10.1007/s10904-023-02957-6.
[23] Z. Guo, Y. Li, S. Zhang, H. Niu, Z. Chen, J. Xu, Enhanced sorption of radiocobalt from water by Bi(III) modified montmorillonite: a novel adsorbent, J. Hazard. Mater. 192 (2011) 168–175, https://doi.org/10.1016/j.jhazmat.2011.05.004.
[24] K. Li, J. Hu, Z. Liu, L. Chen, Y. Dong, Removal of radiocobalt from aqueous solutions by kaolinite affected by solid content, pH, ionic strength, contact time and temperature, J. Radioanal. Nucl. Chem. 295 (2013) 2221–2228, https://doi.org/10.1007/s10967-012-2271-3.
[25] A.F. Seliman, E.H. Borai, Utilization of natural chabazite and mordenite as a reactive barrier for immobilization of hazardous heavy metals, Environ. Sci. Pollut. Res. 18 (2011) 1098–1107, https://doi.org/10.1007/s11356-011-0459-7.
[26] G. Qi, X. Lei, L. Li, C. Yuan, Y. Sun, J. Chen, J. Chen, Y. Wang, J. Hao, Preparation and evaluation of a mesoporous calcium-silicate material (MCSM) from coal fly ash for removal of Co(II) from wastewater, Chem. Eng. J. 279 (2015) 777–787, https://doi.org/10.1016/j.cej.2015.05.077.
[27] D. Humelnicu, M.M. Lazar, M. Ignat, I.A. Dinu, E.S. Dragan, M.V. Dinu, Removal of heavy metal ions from multi-component aqueous solutions by eco-friendly and low-cost composite sorbents with anisotropic pores, J. Hazard. Mater. 381 (2020), https://doi.org/10.1016/j.jhazmat.2019.120980.
[28] J.A. Ricardo-García, Y. Enamorado-Horrutiner, G. Rodríguez-Fuentes, M. S. Pomares-Alfonso, M.E. Villanueva-Tagle, Characterization of zeolite as sorbent for Ni(II) concentration in aqueous solutions, Microchem. J. 164 (2021), https://doi.org/10.1016/j.microc.2021.106064.
[29] Y. Liu, S. Zhao, X. Qiu, Y. Meng, H. Wang, S. Zhou, Q. Qiao, C. Yan, Clinoptilolite based zeolite-geopolymer hybrid foams: potential application as low-cost sorbents for heavy metals, J. Environ. Manag. 330 (2023), https://doi.org/10.1016/j.jenvman.2022.117167.
[30] C. Belviso, P. Lucini, M. Mancinelli, M. Abdolrahimi, A. Martucci, D. Peddis, F. Maraschi, F. Cavalcante, M. Sturini, Lead, zinc, nickel and chromium ions removal from polluted waters using zeolite formed from bauxite, obsidian and their combination with red mud: behaviour and mechanisms, J. Clean. Prod. 415 (2023), https://doi.org/10.1016/j.jclepro.2023.137814.
[31] L. Li, Z. Xu, H. Li, J. Li, D. Hu, Y. Xiang, L. Han, X. Peng, Immobilization of strontium and cesium by aluminosilicate ceramics derived from metakaolin geopolymer-zeolite A composites via 1100 °C heating treatment, Ceram. Int. 48 (2022) 15236–15242, https://doi.org/10.1016/j.ceramint.2022.02.054.
[32] O.O. Shichalin, E.K. Papynov, V.Y. Maiorov, A.A. Belov, E.B. Modin, I.Y. Buravlev, Y.A. Azarova, A.V. Golub, E.A. Gridasova, A.E. Sukhorada, I.G. Tananaev, V. A. Avramenko, Spark plasma sintering of aluminosilicate ceramic matrices for immobilization of cesium radionuclides, Radiochemistry 61 (2019) 185–191, https://doi.org/10.1134/S1066362219020097.
[33] A. Dran'kov, O. Shichalin, E. Papynov, A. Nomerovskii, V. Mayorov, V. Pechnikov, A. Ivanets, I. Buravlev, S. Yarusova, A. Zavjalov, A. Ognev, V. Balybina, A. Lembikov, I. Tananaev, N. Shapkin, Hydrothermal synthesis, structure and sorption performance to cesium and strontium ions of nanostructured magnetic zeolite composites, Nucl. Eng. Technol. 54 (2022) 1991–2003, https://doi.org/10.1016/j.net.2021.12.010.
[34] G.Y. Kim, S.S. Shin, B. Lee, J.H. Choi, H.W. Kang, J.Y. Pyo, J.H. Yang, H.S. Park, K. R. Lee, Characteristics of Cs pollucite synthesized at various Cs loadings for immobilization of radioactive Cs, J. Nucl. Mater. 588 (2024), https://doi.org/10.1016/j.jnucmat.2023.154781.
[35] O.O. Shichalin, E.K. Papynov, N.P. Ivanov, M.I. Balanov, A.N. Dran'kov, A. L. Shkuratov, N.V. Zarubina, A.N. Fedorets, V.Y. Mayorov, A.O. Lembikov, Y. Shi, I. G. Tananaev, A.I. Ivanets, Study of adsorption and immobilization of Cs+, Sr2+, Co2+, Pb2+, La3+ ions on Na-Faujasite zeolite transformed in solid state matrices, Sep. Purif. Technol. 332 (2024), https://doi.org/10.1016/j.seppur.2023.125662.
[36] A.I. Orlova, M.I. Ojovan, Ceramic mineral waste-forms for nuclear waste immobilization, Materials 12 (2019), https://doi.org/10.3390/ma12162638.
[37] O.O. Shichalin, E.K. Papynov, V.A. Nepomnyushchaya, A.I. Ivanets, A.A. Belov, A. N. Dran'kov, S.B. Yarusova, I.Y. Buravlev, A.E. Tarabanova, A.N. Fedorets, S. A. Azon, Z.E. Kornakova, S.Y. Budnitskiy, I.G. Tananaev, Y. Shi, Y. Xiong, H. Wang, Hydrothermal synthesis and spark plasma sintering of NaY zeolite as solid-state matrices for cesium-137 immobilization, J. Eur. Ceram. Soc. 42 (2022) 3004–3014, https://doi.org/10.1016/j.jeurceramsoc.2022.02.007.
[38] A.I. Orlova, M.I. Ojovan, Ceramic mineral waste-forms for nuclear waste immobilization, Materials 12 (2019), https://doi.org/10.3390/ma12162638.
[39] S.B. Yarusova, O.O. Shichalin, A.A. Belov, S.A. Azon, I.Y. Buravlev, A.V. Golub, V. Y. Mayorov, A.V. Gerasimenko, E.K. Papynov, A.I. Ivanets, A.A. Buravleva, E. B. Merkulov, V.A. Nepomnyushchaya, O.V. Kapustina, P.S. Gordienko, Synthesis of amorphous KAlSi3O8 for cesium radionuclide immobilization into solid matrices using spark plasma sintering technique, Ceram. Int. 48 (2022) 3808–3817, https://doi.org/10.1016/j.ceramint.2021.10.164.
[40] E.K. Papynov, A.A. Belov, O.O. Shichalin, I.Y. Buravlev, S.A. Azon, A.V. Golub, A. V. Gerasimenko, Y. Parotkina, A.P. Zavjalov, I.G. Tananaev, V.I. Sergienko, SrAl2Si2O8 ceramic matrices for 90Sr immobilization obtained via spark plasma sintering-reactive synthesis, Nucl. Eng. Technol. 53 (2021) 2289–2294, https://doi.org/10.1016/j.net.2021.01.024.
[41] O.O. Shichalin, S.B. Yarusova, A.I. Ivanets, E.K. Papynov, A.A. Belov, S.A. Azon, I. Y. Buravlev, A.E. Panasenko, P.A. Zadorozhny, V.Y. Mayorov, D.K. Shlyk, V. A. Nepomnyushchaya, O.V. Kapustina, A.E. Ivanova, A.A. Buravleva, E. B. Merkulov, P.S. Gordienko, Synthesis and spark plasma sintering of solid-state matrices based on calcium silicate for 60Co immobilization, J. Alloys Compd. 912 (2022), https://doi.org/10.1016/j.jallcom.2022.165233.
[42] O.O. Shichalin, A.A. Belov, A.P. Zavyalov, E.K. Papynov, S.A. Azon, A.N. Fedorets, I.Y. Buravlev, M.I. Balanov, I.G. Tananaev, Y. Shi, Q. Zhang, M. Niu, W. Liu, A. S. Portnyagin, Reaction synthesis of SrTiO3 mineral-like ceramics for strontium-90 immobilization via additional in-situ synchrotron studies, Ceram. Int. 48 (2022) 19597–19605, https://doi.org/10.1016/j.ceramint.2022.03.068.
[43] G. Wei, X. Liu, S. Chen, D. Shao, W. Yuan, X. Lu, Y. Xie, X. Shu, Direct immobilization of simulated nuclear waste in preformed Gd2Zr2O7 pyrochlore via spark plasma sintering reaction, Mater. Chem. Phys. 291 (2022), https://doi.org/10.1016/j.matchemphys.2022.126711.
[44] E.K. Papynov, O.O. Shichalin, A.A. Belov, I.Y. Buravlev, A.S. Portnyagin, A. G. Kozlov, E.A. Gridasova, I.G. Tananaev, V.I. Sergienko, Ionizing radiation source-open type fabrication using additive technology and spark plasma sintering, Ceram. Int. 49 (2023) 3083–3087, https://doi.org/10.1016/j.ceramint.2022.11.020.
[45] E.K. Papynov, O.O. Shichalin, V.Y. Mayorov, V.G. Kuryavyi, T.A. Kaidalova, L. V. Teplukhina, A.S. Portnyagin, A.B. Slobodyuk, A.A. Belov, I.G. Tananaev, V. A. Avramenko, V.I. Sergienko, SPS technique for ionizing radiation source fabrication based on dense cesium-containing core, J. Hazard. Mater. 369 (2019) 25–30, https://doi.org/10.1016/j.jhazmat.2019.02.016.
[46] P.S. Gordienko, V.V. Bagramyan, S.B. Yarusova, A.A. Sarkisyan, G.F. Krysenko, N. V. Polyakova, Y.V. Sushkov, Effect of microwave treatment on the kinetics of formation and morphology of calcium hydrosilicates, Russ. J. Appl. Chem. 85 (2012) 1519–1523, https://doi.org/10.1134/S1070427212100059.
[47] P.S. Gordienko, S.B. Yarusova, I.Y. Buravlev, I.G. Zhevtun, Studying the kinetics of the alkaline processing of boron production wastes under different conditions, Russ. J. Phys. Chem. A 95 (2021) 38–42, https://doi.org/10.1134/S003602442101009X.
[48] S.B. Yarusova, P.S. Gordienko, A.A. Yudakov, Y.A. Azarova, R.D. Yashchuk, Kinetics of the sorption of heavy-metal ions by a sorbent obtained from boric acid production waste, Theor. Found. Chem. Eng. 50 (2016) 841–845, https://doi.org/10.1134/S0040579516050250.
[49] J.Y. Lin, N.N.N. Mahasti, Y.H. Huang, Recent advances in adsorption and coagulation for boron removal from wastewater: a comprehensive review, J. Hazard. Mater. 407 (2021), https://doi.org/10.1016/j.jhazmat.2020.124401.
[50] T. Kütük-Sert, S. Kütük, Physical and Marshall Properties of Borogypsum Used as Filler Aggregate in Asphalt Concrete, 2013, https://doi.org/10.1061/(ASCE)MT.1943.
[51] C.B. Emrullahoglu Abi, Effect of borogypsum on brick properties, Constr. Build. Mater. 59 (2014) 195–203, https://doi.org/10.1016/j.conbuildmat.2014.02.012.
[52] Y.Y. Çelen, A. Evcin, I. Akkurt, N. Bezir, K. Günoğlu, N. Kutu, Evaluation of boron waste and barite against radiation, Int. J. Environ. Sci. Technol. 16 (2019) 5267–5274, https://doi.org/10.1007/s13762-019-02333-3.
[53] Y.Y. Çelen, A. Evcin, Synthesis and characterizations of magnetite-borogypsum for radiation shielding, Emerg. Mater. Res. 9 (2020) 770–775, https://doi.org/10.1680/jemmr.20.00098.

[54] U.K. Sevim, M. Ozturk, S. Onturk, M. Balcikanli Bankir, Utilization of boron waste borogypsum in mortar, J. Build. Eng. 22 (2019) 496–503, https://doi.org/10.1016/j.jobe.2019.01.015.
[55] H. Ansari, A.A. Oladipo, M. Gazi, Alginate-based porous polyHIPE for removal of single and multi-dye mixtures: competitive isotherm and molecular docking studies, Int. J. Biol. Macromol. 246 (2023), https://doi.org/10.1016/j.ijbiomac.2023.125736.
[56] K. Suwannahong, S. Wongcharee, T. Kreetachart, C. Sirilamduan, J. Rioyo, A. Wongphat, Evaluation of the microsoft excel solver spreadsheet-based program for nonlinear expressions of adsorption isotherm models onto magnetic nanosorbent, Appl. Sci. (Switzerland) 11 (2021), https://doi.org/10.3390/app11167432.
[57] B. Subramanyam, A. Das, Linearised and non-linearised isotherm models optimization analysis by error functions and statistical means. http://www.ijehse.com/content/12/1/92, 2014.
[58] S.B. Yarusova, O.O. Shichalin, A.A. Belov, S.A. Azon, I.Y. Buravlev, A.V. Golub, V. Y. Mayorov, A.V. Gerasimenko, E.K. Papynov, A.I. Ivanets, A.A. Buravleva, E. B. Merkulov, V.A. Nepomnyushchaya, O.V. Kapustina, P.S. Gordienko, Synthesis of amorphous KAlSi3O8 for cesium radionuclide immobilization into solid matrices using spark plasma sintering technique, Ceram. Int. 48 (2022) 3808–3817, https://doi.org/10.1016/j.ceramint.2021.10.164.
[59] O. Cherkas, T. Beuvier, F. Zontone, Y. Chushkin, L. Demoulin, A. Rousseau, A. Gibaud, On the kinetics of phase transformations of dried porous vaterite particles immersed in deionized and tap water, Adv. Powder Technol. 29 (2018) 2872–2880, https://doi.org/10.1016/j.apt.2018.08.008.
[60] K. Zheng, X. Xie, G. Gou, X. Chen, Y. Huang, J. Gao, Comparative study on characteristics and microstructure of magnesium silicate hydrate utilizing quartz and silica fume as siliceous raw materials, Case Stud. Constr. Mater. 19 (2023), https://doi.org/10.1016/j.cscm.2023.e02313.
[61] A. Mahmood, A. Ibuk, M. Vogel, C. Neuhaus, F. Dehn, P. Thissen, Unraveling carbonation and CO2 capture in calcium-silicate-hydrate, ACS Sustain. Chem. Eng. 11 (2023) 13002–13012, https://doi.org/10.1021/acssuschemeng.3c02469.
[62] S. Arul raja sekaran, K.A. Naseer, K. Marimuthu, N. Almousa, M.I. Sayyed, Investigations on physical, structural, elastic, optical and radiation shielding properties of calcium phospho-silicate glasses, Radiat. Phys. Chem. 214 (2024), https://doi.org/10.1016/j.radphyschem.2023.111306.
[63] T. Ivory-Cousins, A. Nurzynska, K. Klimek, D.K. Baines, W. Truszkiewicz, K. Pałka, T.E.L. Douglas, Whey protein isolate/calcium silicate hydrogels for bone tissue engineering applications—preliminary in vitro evaluation, Materials 16 (2023), https://doi.org/10.3390/ma16196484.
[64] A. de P. Melo, C.M.P. de Rosatto, D.C. Ferraz, G.L. de Souza, C.C.G. Moura, Evaluation of cytotoxicity, cell attachment, and elemental characterization of three calcium silicate-based sealers, Materials 16 (2023), https://doi.org/10.3390/ma16206705.
[65] M.K.A. Lafmejani, A. Parsa, M. Mirmohammadi, T. Ahmadi, H. Mirmohammadi, A novel and facile synthesis of calcium silicate nanoparticles as a base for root canal cement/sealer under constant potential: compared to chemical synthesis, Mater. Chem. Phys. 315 (2024), https://doi.org/10.1016/j.matchemphys.2024.128924.
[66] J. Mokrzycki, P. Baran, M. Gazda-Grzywacz, J. Bator, W. Wróbel, K. Zarębska, Decarbonatization of energy sector by CO2 sequestration in waste incineration fly ash and its utilization as raw material for alkali activation, Materials 16 (2023), https://doi.org/10.3390/ma16186094.
[67] A.S. Elshimy, H.A. Abdel-Gawwad, M. Al-Dossari, N.S. Abd EL-Gawaad, A. Bonilla-Petriciolet, M. Badawi, M. Mobarak, E.C. Lima, A.Q. Selim, M.K. Seliem, Utilization of alkali-activated dolomite waste toward the fabrication of an effective adsorbent: experimental study and statistical physics formalism for the removal of methylene blue and crystal violet, J. Phys. Chem. Solids 180 (2023), https://doi.org/10.1016/j.jpcs.2023.111442.
[68] J.A. Pérez-Casas, A.A. Zaldívar-Cadena, A. Álvarez-Mendez, J.J. Ruiz-Valdés, S. M. de la Parra-Arciniega, D.C. López-Pérez, A.I. Sánchez-Vázquez, Sugarcane bagasse ash as an alternative source of silicon dioxide in sodium silicate synthesis, Materials 16 (2023), https://doi.org/10.3390/ma16186327.
[69] A. Godelitsas, J.M. Astilleros, Dissolution, sorption/(re)precipitation, formation of solid solutions and crystal growth phenomena on mineral surfaces: implications for the removal of toxic metals from the environment, Eur. Mineral. Union Notes Mineral. 10 (2010) 289–324, https://doi.org/10.1180/EMU-notes.10.8.
[70] A.R. Lucaci, D. Bulgariu, I. Ahmad, G. Lisa, A.M. Mocanu, L. Bulgariu, Potential use of biochar from variouswaste biomass as biosorbent in Co(II) removal processes, Water (Switzerland) 11 (2019), https://doi.org/10.3390/w11081565.
[71] M. Pipíška, E. Florková, P. Nemeček, L. Remenárová, M. Horník, Evaluation of Co and Zn competitive sorption by zeolitic material synthesized from fly ash using 60 Co and 65 Zn as radioindicators, J. Radioanal. Nucl. Chem. 319 (2019) 855–867, https://doi.org/10.1007/s10967-018-6390-3.
[72] J. Bąk, P. Thomas, D. Kołodyńska, Chitosan-modified biochars to advance research on heavy metal ion removal: roles, mechanism and perspectives, Materials 15 (2022), https://doi.org/10.3390/ma15176108.
[73] G. Qi, X. Lei, L. Li, C. Yuan, Y. Sun, J. Chen, J. Chen, Y. Wang, J. Hao, Preparation and evaluation of a mesoporous calcium-silicate material (MCSM) from coal fly ash for removal of Co(II) from wastewater, Chem. Eng. J. 279 (2015) 777–787, https://doi.org/10.1016/j.cej.2015.05.077.
[74] N.J. Coleman, D.S. Brassington, A. Raza, A.P. Mendham, Sorption of Co2+ and Sr2+ by waste-derived 11 Å tobermorite, Waste Manag. 26 (2006) 260–267, https://doi.org/10.1016/j.wasman.2005.01.019.
[75] W. Qiu, Y. Zheng, Removal of lead, copper, nickel, cobalt, and zinc from water by a cancrinite-type zeolite synthesized from fly ash, Chem. Eng. J. 145 (2009) 483–488, https://doi.org/10.1016/j.cej.2008.05.001.
[76] A. Ahmadpour, M. Tahmasbi, T.R. Bastami, J.A. Besharati, Rapid removal of cobalt ion from aqueous solutions by almond green hull, J. Hazard. Mater. 166 (2009) 925–930, https://doi.org/10.1016/j.jhazmat.2008.11.103.
[77] S. Mignardi, L. Archilletti, L. Medeghini, C. De Vito, Valorization of eggshell biowaste for sustainable environmental remediation, Sci. Rep. 10 (2020), https://doi.org/10.1038/s41598-020-59324-5.
[78] M. Xiao, Y. Wei, P. Zhang, The effect of sintering temperature on the crystal structure and microwave dielectric properties of CaCoSi 2 O 6 ceramic, Mater. Chem. Phys. 225 (2019) 99–104, https://doi.org/10.1016/j.matchemphys.2018.12.027.